

LOW-LEVEL INFLOW PATTERNS TO TROPICAL CYCLONES AS DETERMINED
WITH GLOBAL POSITIONING SYSTEM DROPWINDSONDES

A THESIS SUBMITTED TO THE GRADUATE DIVISION OF THE
UNIVERSITY OF HAWAI'I AT MĀNOA IN PARTIAL FULFILLMENT
OF THE REQUIREMENTS FOR THE DEGREE OF

MASTER OF SCIENCE

IN

METEOROLOGY

DECEMBER 2010

By

Julie K. Kelly

Thesis Committee:

Gary M. Barnes, Chairperson

Thomas A. Schroeder

Richard Knabb

Acknowledgements

I would like to thank Dr. Gary Barnes for his dedication of time, patience and knowledge towards the direction and improvements of my thesis. I would not have been able to this without your creativity and criticism. I would also like to thank my committee members Dr. Tom Schroeder and Dr. Rick Knabb for their guidance and comments through out the process.

I extend a special thank you to soon-to-be Dr. Klaus Dolling for his invaluable computer program used in this study and many hours of guidance. Also, I thank Aaron Levine for his patience and programming knowledge. Mahalo to my fellow graduate students for helping me stay focused on my goals and keeping my sanity along the way.

Abstract

Data collected with Global Positioning System dropwindsondes (GPS sondes) in four tropical cyclones (TCs) are analyzed to determine how the low-level inflow varies azimuthally and in thickness. The structure of a developing tropical cyclone is highly asymmetric and is influenced by two key factors: vertical shear of the horizontal wind and storm motion. Composites from GPS sondes were supplemented with aircraft radar and the Hurricane Research Division's H*wind analysis to produce horizontal plan view images of the radial flow at varying heights. Inflow depths were also plotted as a function of latitude and longitude.

This study provides evidence that as a TC intensifies, the inflow depth decreases and the inflow becomes more axisymmetric. The vertical structure was found to remain nearly unchanged within a 100 km annulus of the storm center, in the lowest 1 km for the weaker TCs, while the two major hurricanes showed significant changes in the radial speed, depth and azimuthal coverage around the storm center. The wind shear and the storm motion were found to influence maximum inflow location and appear to be correlated with boundary layer asymmetries in the radial flow. This is in accordance with previous studies from Corbosiero and Molinari. The angle between the TC motion and the wind shear vectors appears to influence the magnitude of the inflow velocities. When the TC motion vector lies to the left of the wind shear vector and the angle between them is less than 135 degrees, then both factors predict inflow maxima collocated in the same region.

Table of Contents

Acknowledgements.....	i
Abstract.....	ii
List of Tables	v
List of Figures.....	vi
Chapter 1 Introduction.....	1
1.1 Background.....	1
1.2 History	4
1.2.1 Asymmetry	4
1.2.2 Environmental Shear	6
1.2.3 Motion.....	6
1.3 Hypotheses.....	9
Chapter 2 Data and Analysis Methods	11
2.1 Data.....	11
2.2 Analysis Methods	17
Chapter 3 Results.....	20
3.1 Horizontal Analysis	20
3.2 Vertical Analysis	28
3.3 Harmonic Analysis	31
Chapter 4 Discussion	33
4.1 The Relationship between Motion and VWS	33
Chapter 5 Summary and Model Discussion	38

5.1 Summary.....	38
5.2 Model Discussion	42
Chapter 6 Future Work.....	44
References.....	46

List of Tables

<u>Table</u>	<u>Page</u>
1. Number of GPS sondes available for analysis at each level	12
2. Storm details for the 18 UTC record based upon Best Track..... and SHIPS reanalysis data.	13
3. Portion of variance for wave number 1 (w1) and wave..... number 2 (w2) harmonics for each case.	31

List of Figures

<u>Figure</u>	<u>Page</u>
1. Horizontal Distribution of GPS sondes at 50 m	49
2. Radial contours (m s^{-1}) for Gabrielle 9/15	50
3. Radar image for Gabrielle 9/15	51
4. 500 m tangential contours (m s^{-1}) for Gabrielle 9/15	51
5. Radial contours (m s^{-1}) for Gabrielle 9/16	52
6. Radar image for Gabrielle 9/16	53
7. 500 m tangential contours (m s^{-1}) for Gabrielle 9/16	53
8. Radial contours (m s^{-1}) for Humberto 9/23	54
9. Radar image for Humberto 9/23	55
10. 500 m tangential contours (m s^{-1}) for Humberto 9/23	55
11. Radial contours (m s^{-1}) for Isidore 9/21	56
12. Radar Image for Isidore 9/21	57
13. 500 m tangential contours (m s^{-1}) for Isidore 9/21	57
14. Radial contours (m s^{-1}) for Rita 9/21	58
15. Radar Image for Rita 9/21	59
16. 500 m tangential contours (m s^{-1}) for Rita 9/21	59
17. Radial contours (m s^{-1}) for Rita 9/22	60
18. Radar Image for Rita 9/22	61
19. 500 m tangential contours (m s^{-1}) for Rita 9/22	61
20. Inflow depths (m)	62
21. Radial flow around the RMW at 150 m	63

22. Inflow relative to the VWS and Motion vectors.....	64
--	----

Chapter 1

Introduction

1.1 Background

Low-level inflow in tropical cyclones (TCs) is a vital component of the secondary circulation. Inflow is responsible for importing angular momentum and thermal energy into a storm (Ooyama 1982, Riehl and Malkus 1961). Ooyama (1982) stated that the intensification of a TC, that is an increase in the maximum sustained winds within the eyewall, is only possible when a deep inflow layer is established. A deep inflow layer would, in theory, import more angular momentum into a vortex allowing for rotational velocities to increase. On the other hand, an inflow layer that exceeds the depth of the boundary layer would also import lower moist entropy air into the eye wall, thus inhibiting convection and affecting the intensification of the surface circulation by decreasing latent heat release aloft. As a TC matures, the inflow rate, depth, and azimuthal extent will likely vary. Therefore, mapping the low-level inflow as a function of TC intensity may reveal features associated with formation, when the TC forms a warm core, and intensification when the TC achieves high Saffir-Simpson category. Understanding the inflow to a TC throughout its life cycle may help to improve model forecasts, help to provide better guidance to the public and possibly reduce costs from low confidence forecasts that result in over-warning and unnecessary evacuation.

Previous studies have examined the structure of the low-level inflow in TCs based on observations (Frank 1977, Kaplan and Frank 1993, Schneider and Barnes 2005, Kepert 2006a, b, Sitkowski and Barnes 2009). While these studies have broken ground and begun to paint a picture of radial and tangential flow fields, there has not been a

study concentrated on measuring the asymmetry and depth of the inflow for TCs of varying intensities. Another topic of debate among earlier investigators has been how storm motion and vertical shear of the horizontal wind (hereafter known as VWS) impact the asymmetry of the inflow (Black et al. 2002, Reasor et al. 2000, Bender 1997, DeMaria 1996).

Analyzing TC or vortex scale features over short periods requires a decent amount of in-situ observations which are hard to acquire when a TC develops in data sparse regions far from land-based observing stations. Synoptic scale weather patterns can be derived from a compilation of satellite and radar imagery, networks of surface and upper air observations, and occasional ship and buoy reports. Vortex scale features are often observed through aircraft reconnaissance. These flights investigate storms for a period of 3-8 hours. Aircraft can provide researchers with flight level winds (which can be derived down to near surface), radar, and dropwindsondes. Deploying dropwindsondes from aircraft is a reliable way to map multiple levels of a storm at either synoptic or meso-gamma scales. The sampling density of the drops limits the horizontal resolution of the composite and varies from one storm to another based on multiple factors such as flight pattern, storm location, and overall mission.

Deploying dropwindsondes to analyze the state of the atmosphere was first employed during the Global Atmospheric Research Program Atlantic Tropical Experiment (GATE) in the summer of 1974 (Govind 1975). Afterwards, researchers saw the potential benefits for releasing the dropwindsondes into tropical cyclones. This allowed for more data to be collected while the storm was still over open waters and in certain cases allowed for a limited view of storm evolution. The dropwindsonde itself has

evolved into the modern day Global Positioning System dropwindsondes (GPS sondes). The use of these GPS sondes in TCs has allowed an increase in vertical resolution, providing data about every 7 meters during its descent to the surface. This sampling method allows for researchers to have a better view of kinematic and thermodynamic structures in TCs.

1.2 History

1.2.1 Asymmetry

Frank (1977) presented one of the first views of the general structure of a typhoon. He used what observational data were available in the Northwest Pacific at the time. His composites were composed over a 10-year timescale from 7,784 soundings launched at 30 stations into mature typhoons. His cross-sectional analysis showed asymmetries in the radial flow with maximum inflow values to the right of the motion or the east quadrant. Kaplan and Frank (1993) (hereafter KF93) advanced the field with their research of Hurricane Frederic (1979). The duo used observations from five sources over roughly 48 hours to produce composites of the secondary flow fields. Utilizing cloud motion winds (CMW's), rawinsondes, buoys, ships, and aircraft data, they constructed plan views of the large-scale radial flow. However, Frederic underwent a rapid intensification (RI) cycle during the analysis period going from a CAT 1 to a CAT 4 hurricane. Even though the structures from each stage of the TC's life cycle were smoothed out during compositing, the results still showed asymmetries in the radial flow near the surface. KF93 had more data to use within a degree latitude of the circulation center at multiple levels than Frank did for his first work, but they were still lacking data from inside the TC. Important features are averaged out when one composites over a large time scale; and for a TC, which is constantly evolving, 48 hours is a very long period to composite.

Perhaps, had KF93 done a composite before RI and one after, a transition to a more axisymmetric inflow around the vortex would have been observed. This was the case with Sitkowski and Barnes' (2009) work with the RI of Hurricane Guillermo (2003).

The data set consisted of 70 GPS sondes deployed from two of NOAA's WP-3D aircraft on two consecutive days. Plan view images of the radial flow composited before rapid intensification showed strong asymmetries in the low-levels. On the first day of analysis, strong asymmetries were observed at 100 m with the maximum inflow located downshear or to the southeast of the storm's center. Analysis conducted after RI, when the storm deepened 25 hPa, shows a shift towards more axisymmetric inflow at the same level, and there were no significant changes in the VWS. These findings illustrate that the radial flow can undergo drastic changes with intensification and that further research is needed to: 1) understand the evolution of the inflow throughout a TCs' life cycle and 2) determine how low-level fields are modulated by storm motion and/or environmental wind shear.

Kepert (2006a, b) examined the low-level kinematic structure of two intense hurricanes, Georges (1998, 939 hPa) and Mitch (1998, 930 hPa intensity during sampling) with GPS sondes. Both TCs exhibited strong inflow often exceeding -30 m s^{-1} near the eyewall and an inflow depth that was frequently shallow, usually about 1 km deep. Georges, moving at over 7 m s^{-1} , had strong inflow on its' front quadrants and right rear quadrant. Inflow existed completely around the storm until 1000 m altitude where weak outflow in a wave number one pattern became apparent. Mitch, moving at just over 2 m s^{-1} , had its' strongest inflow on the left side and had outflow by 500 m altitude. Kepert (2006b) argued that the nearness to land was the cause of the inflow asymmetry.

1.2.2 Environmental Shear

Numerous studies have touted the negative effects of VWS on a TC (DeMaria and Kaplan 1994, Black et al. 2002, Corbosiero and Molinari 2002, Kaplan and DeMaria 2003, Knaff et al. 2004). In the aforementioned studies, VWS was stated to be a primary forcing for asymmetries in the convective structure of a TC. Peng et al. (1999) showed that the introduction of uniform environmental flow onto an existing vortex resulted in the slowing of intensification and weakening of a storm primarily from the development of asymmetries in the convection. As a response to VWS, a dipole in vertical motions will develop around a vortex leading to ascent downshear and descent upshear (Raymond 1992, Raymond and Jiang 1990). Bender (1997) provided further support for the negative effect of asymmetrical convergence around a vortex under the effects of shear. Observational studies support this notion (Corbosiero and Molinari 2002, Molinari et al. 2006, Heymsfield et al. 2006, Black et al. 2002) through the observed maxima in radar reflectivities and lightning activity being located left of downshear. Bender (1997) also stated that VWS influenced radar reflectivity structure more than asymmetrical surface friction. What impact does VWS have on the depth, magnitude and location of the inflow? The GPS sondes deployed in TCs of varying intensity will further our understanding of why TCs in shear tend to have asymmetrical reflectivity and vertical velocity fields.

1.2.3 Motion

A translating TC will have stronger winds to the right of motion and weaker winds to the left, relative to the earth. These asymmetries in the wind field force

asymmetries in the boundary layer frictional drag and therefore convergence (Shapiro 1983). As stated in the previous section for VWS, asymmetries in convergence results in asymmetries in convection, ergo asymmetries in radial flow. Powell (1982) showed a relationship between storm motion and convection in Hurricane Frederic (1979), where he found the isotach maximum to be ahead of the storm. Shapiro (1983) compared Hurricanes Allen (1980) and Frederic to his boundary layer slab model results to support that convergence, and therefore inflow, is at a maximum ahead of the storm due to the motion. For Frederic, with a motion of 5 m s^{-1} , reflectivity returns implied a convergence maximum in the right front quadrant. For Allen, whose storm motion was nearly double that of Frederic, the convergence maximum was directly ahead of the storm. These observations confirmed his model simulations. Frank and Ritchie's (1999) simulations of a vortex in dry and moist conditions showed similar findings in the shift of the convergence maximum locale as a response to an increase in translation velocity. Kepert (2006a) showed for fast-moving Georges (1998) maximum inflow was found on the leading edge side, and the right rear quadrant. The strong inflow in the right rear quadrant was not due to the presence of a mesovortex, but its' exact cause remained uncertain.

Motion and VWS have been presented as individual forcing mechanisms for boundary layer asymmetries. However, in reality, they both influence TCs and the two forces interacting with each other can influence kinematic structures. In particular, which factor is more dominant in producing low-level asymmetries, storm motion or VWS? For the case of motion and VWS acting together, as stated above by Bender (1997), VWS was shown to influence boundary layer asymmetries more than storm motion (Frank and

Ritchie 1999, Corbosiero 2000, Corbosiero and Molinari 2003). The inflow data from the GPS sondes, combined with the storm motion derived from the aircraft center fixes, can be used to examine the relationship between inflow traits and storm motion.

1.3 Hypotheses

In this study I will analyze low-level radial flow fields and evaluate the changes with intensity. Four storms of varying intensity, ranging from tropical storm to CAT 5 hurricane, will be analyzed. The data are comprised of GPS sondes deployed from National Oceanic and Atmospheric Administration (NOAA) and United States Air Force reconnaissance aircraft. The storms were chosen based on the number of drops in and around the circulation center of the storm. A minimum of 20 sondes per day, after quality controls, was set. The storms chosen were Tropical Storm Gabrielle (2001), Hurricane Humberto (2001), Hurricane Isidore (2002), and Hurricane Rita (2005). The hypotheses for this study are as follows:

- (1) As TCs intensify the inflow becomes:
 - (a) more axisymmetric,
 - (b) the magnitude of the radial speed increases, and
 - (c) the depth of the inflow decreases.

This is due to the increase in subsidence as the eyewall becomes better organized and convection increases around the core with increasing intensity. The increase in subsidence will act to lower the inflow depth.

- (2) The two key factors that impact the magnitude and degree of asymmetry of the inflow are:

- (a) the VWS, and
- (b) TC motion.

Here I expect the leading edge side of the vortex of a fast-moving TC to have the strongest inflow. Deep convection as shown by the reflectivity field shows that down

shear left is the most active part of a TC. I expect to see the strongest inflow in that quadrant that is left and down shear.

Chapter 2 Data and Analysis Methods

2.1 Data

GPS sondes

GPS sondes with a vertical resolution of about 7 meters provide data from a few hundred meters below flight level to less than 10 m from the sea surface in most cases. This is an improvement from previous versions of dropwindsondes, which rarely provided wind data below 400 m (Hock and Franklin 1999). Resolution for pressure, temperature, relative humidity, and wind speed with the GPS sondes are all 0.1 for their respective units. Accuracies of the aforementioned variables are 0.2hPa, 0.2 C, 2%, and 0.5 m s^{-1} , respectively (Hock and Franklin 1999). All GPS sondes were quality controlled by processing the raw data through the Atmospheric Sounding Processing Environment (ASPEN) software developed by the National Center for Atmospheric Research (NCAR) to read Airborne Vertical Atmospheric Profiling System (AVAPS) files ([http:// www.eol.ucar.edu/rtf/facilities/software/aspn/Aspen%20Manual.pdf](http://www.eol.ucar.edu/rtf/facilities/software/aspn/Aspen%20Manual.pdf)). Further quality control of the data will be discussed in the composite analysis section. Table 1 depicts the GPS sondes available for composite analysis at each level.

	50 m	150 m	500 m	1 km	2 km	3 km
Gabrielle 9/15	30	30	30	30	30	30
Gabrielle 9/16	23	23	23	23	23	21
Humberto 9/23	52	53	55	52	31	31
Isidore 9/21	55	60	62	53	N/A	N/A
Rita 9/21	50	56	57	56	N/A	N/A
Rita 9/22	49	56	56	54	N/A	N/A

Table 1. Number of GPS sondes available for analysis at each level.

Wind Shear

VWS data are from the Statistical Hurricane Intensity Prediction Scheme (SHIPS, Kaplan and DeMaria 1995, DeMaria and Kaplan 1994) operational reanalysis data set with 2009 modifications for the Atlantic. Atmospheric predictors for 6-hour intervals are from the National Centers for Environmental Prediction's (NCEP) operational global model analyses, plus satellite data when available. The 18 UTC initial VWS magnitude and direction were used for all storms, as this time coincided with the period of flight reconnaissance. The wind shear is calculated by taking the layer between 850 and 200 hPa around a 2° to 8° annulus relative to storm center.

Storm Track

Center positions were obtained by a compilation of Best Track and flight fixes for the period during aircraft investigation. The Best Track data set can be obtained online through the National Hurricane Center's (NHC) online archives (<http://www.nhc.noaa.gov>). Flight fixes from NOAA's WP-3D aircraft were obtained

from the Hurricane Research Division (HRD). Storm motion and translation speed were calculated using these center fixes. Central pressures and maximum sustained winds were also from the NHC’s online archive. Table 1 shows the intensity, motion and shear for each day of analysis.

	MSLP (mb)	V max (m/s)	Motion (deg, m/s)	Shear (deg, m/s)	Category
Gabrielle 9/15/01	999	23	59 8.9	43 14	TS
Gabrielle 9/16/01	995-991	28	41 11	50 18	TS
Humberto 9/23/01	986-983	41	23 7.8	42 10	CAT 1
Isidore 9/21/02	946	57	300 2.3	146 5	CAT 3
Rita 9/21/05	920-897	75	283 4.2	39 3	CAT 4/5
Rita 9/22/05	914	80	300 4.3	120 4	CAT 5

Table 2. Storm details for the 18 UTC record based upon Best Track and SHIPS reanalysis data. For Gabrielle 9/16, Humerto, and Rita 9/21, the range in the MSLP is the change between 18 to 00 UTC.

Gabrielle (2001)

Analyses for Gabrielle were performed for September 15 and 16, when the storm entered the Atlantic after making landfall along the Gulf coast of Florida. The storm was investigated for approximately 5.5 hours on the 15th with the first drop at 1859 UTC. Thirty-three GPS sondes were deployed from the NOAA-42 aircraft. After processing through ASPEN, 30 sondes were used for compositing. Data were available for 100% of this set from 3 km to 50 m. Figure 1a depicts the horizontal distribution of the GPS sondes at 50 m. Due to the flight pattern, there are no drops in the northeast quadrant on this day of analysis. The storm’s median position for this time was 30.16°N, 78.10°W at 2032 UTC and the central pressure remained constant at 995 hPa over the period of

analyses, while the maximum sustained winds were 23 m s^{-1} . Gabrielle experienced strong southwesterly VWS of 13.5 m s^{-1} and was moving at 9 m s^{-1} to the northeast, almost double the average speed for a TC. During this time, Gabrielle began to interact with a mid-latitude cyclone that was moving off the east coast. Over the two days this trough was responsible for the increase in 5 m s^{-1} of VWS and 2 m s^{-1} in the translational speed of the TC. After quality controls were performed, 23 drops were used in compositing with 93% of the data available from 50 m to 2 km and 84% for 3 km. There is only one drop in the center on this day of analysis.

Humberto (2001)

Hurricane Humberto never made landfall, but was one of the most sampled storms in the Atlantic. For purposes of this study, I am analyzing data on September 23 from two NOAA aircraft. Humberto was investigated for approximately 4 hours with the deployment of 71 GPS. After processing in ASPEN, 67 sondes were used in compositing with roughly 76% of the data available from 50 m to 1 km. There are no data above 1 km from the NOAA-43 plane. Humberto was centered at 32.74°N , 67.08°W at the median time of 2231 UTC. The storm was moving to the northeast at nearly 8 m s^{-1} and was embedded in moderate VWS of approximately 10 m s^{-1} . The central pressure was 986 hPa at 1800 UTC and had decreased by 9 hPa since 0000 UTC on the 23rd, attaining hurricane strength on this day. The maximum sustained winds were 41 m s^{-1} , also at 18 UTC. Humberto peaked in intensity on the 24th at 0000 UTC, near the end of the flight reconnaissance, with a minimum pressure of 983 hPa.

Isidore (2002)

Isidore was a tropical cyclone for 13 days, made three landfalls and was responsible for 7 deaths in all. On September 23rd, Isidore reached its maximum intensity with 57 m s^{-1} maximum sustained winds and a central pressure of 946 hPa. This study focuses on data collected during reconnaissance on September 21 when Isidore, as a category 3 hurricane, was moving at a nominal speed of 2 m s^{-1} to the west-northwest in the western Caribbean and experiencing moderate northwesterly shear of 6 m s^{-1} . NOAA aircraft dropped 73 sondes and 69 of those were used in compositing. Roughly 87% of the post-processed sondes were available at all levels for analysis.

Rita (2005)

Rita rapidly intensified from a tropical storm to a category 5 hurricane in 36 hours as the warm waters from the Gulf's loop current aided in intensification. Rita reached category 5 status on September 21, the first day of analysis. VWS was a moderate 6 m s^{-1} from the southwest and had a translational speed of 4 m s^{-1} to the west-northwest. NOAA and Air Force flights launched a combined 74 sondes into Rita. While, there are drops from within the eye, there are no drops for 100 km to the southeast of the center. Sixty-one of those sondes survived ASPEN quality controls and 95% of those were available for 150 m to 1 km heights. The availability decreases at 50 m to 86% of the sondes providing data. There are no GPS sondes directly to the southeast of the center on this day of analysis. On the second day of analysis, September 22, Rita reached its maximum intensity with a central pressure of 897 hPa and maximum sustained winds of 80 m s^{-1} . The VWS had increased to 7 m s^{-1} while the motion stayed constant. Seventy-four

sondes were launched on this day from Air Force and NOAA aircraft. Fifty-nine sondes were used in compositing with 95% of the data available for all levels.

2.2 Analysis Methods

Composites

Composite images of the tangential (V_t) and radial (V_r) fields produced from the quality controlled GPS sondes are storm relative and are centered around a median time calculated from the first to the last drop of the day. These data were interpolated vertically to intervals of 10 m. Horizontal plan view images were produced using a cubic-spline method (Dolling 2010) to preserve the observed values of the data at their observed location. While most analyses proved to be accurate when compared to subjective hand analyses, some unrealistic features develop in data sparse areas. Due to the horizontal distribution of the GPS sondes, only octant to quadrant features can be resolved. The three cases this affected most significantly are Gabrielle September 15, Gabrielle September 16, and Rita September 21. The most common problem was the creation of a false maximum or minimum in the radial flow in a quadrant with very few drops. Analyses of the tangential flow proved to be slightly more unrealistic for the aforementioned cases. The circular pattern in the flow was not captured very well due to the inability for the cubic-spline to interpolate in a circular pattern in data sparse regions. For these cases, the tangential flow fields have been smoothed by hand analysis and supplemented with radar and H*wind analysis fields, supplied by HRD.

Inflow depths were plotted as a function of latitude and longitude by analyzing individual sondes. The top of the inflow depth was determined to be the level at which the flow crossed the zero line and became outflow on a plot of radial velocity versus height. If a profile exhibited outflow in the lowest levels it was set to a height of zero. For profiles where the radial inflow was greater than -5 m s^{-1} at 3 km, inflow depths were set

to be greater than 3 km in the contours for Gabrielle and Humberto. The maximum level of analysis for Isidore and Rita was 1 km, therefore any profiles where the radial flow exceeded -5 m s^{-1} at 1 km were set to be greater than 1 km. If the data ceased before the flow crossed the zero line, then a linear fit was applied to the profile to determine the inflow depth only if 1) the last value of radial flow was -7 m s^{-1} or less and 2) the extrapolation was for a layer of 500 m or less. Profiles that were missing more than half of the data were not included in the plots. Since the two major hurricanes do not have data above 1 km, I will analyze the area within a 100 km annulus of the core to determine if the inflow depth is indeed decreasing with an increasing intensity. Here I expect to see depths below 1 km around the core in the strongest storms. Therefore, the lack of data above 1 km in the two major hurricanes will not affect this part of the analysis.

Harmonic Analysis

Harmonic analysis was performed on the 50 m radial flow for all composites in order to quantify the change in asymmetry with increasing intensity. Four radii were chosen for this objective: 1) a distance at 5 kilometers inside the radius of maximum winds (RMW), 2) RMW, 3) one and one-half the distance of the RMW, and 4) two times the distance of the RMW. Sixteen points, at $\pi/8$ intervals, were included in the computations for wave numbers 1 and 2. If a point at a given radius was located at a distance beyond the range of the interpolated data, then an analysis was not performed at that distance. This is the case for the outermost range for Gabrielle on September 16. The southern portion of the two outer radii had three points that were outside of the data grid and therefore harmonic analyses are only available just inside the RMW and at the RMW. Analyses follow standard methods, which are covered thoroughly in Wilks

(2005). Portions of variance (R^2) for a given harmonic are calculated and used as an indicator for a change in asymmetry at a given radius, similar to the analyses performed by Black and Anthes (1971) on quantifying asymmetries in outflow. The equations for the Fourier Transform are not capable of detecting the energy for wave number 0. Wave number 2 is the lowest harmonic that can be analyzed this method that detects the symmetric component of the storm.

Chapter 3

Results

3.1 Horizontal Analysis

Gabrielle:

The convective bands of a tropical storm are usually 50 km or more away from the nascent circulation center, have an asymmetric distribution around the center and are far shorter-lived than the eyewall of a mature hurricane (Riehl 1954). This appears to be the case for the radial flow in Gabrielle that would support the convective bands. The 50 m plan view image of radial flow for September 15 presents an asymmetric field with the sharpest gradients located about 100 km to the northwest of the low-level circulation center (LLCC) (Figure 2a). Near zero flow is observed within a 50 km radius of the core. The maximum inflow at this level, -15 m s^{-1} , is located 280 km northwest of the LLCC. Complementary outflow, reaching maximum values of 20 m s^{-1} , are observed 140 km due west of the LLCC. The radial structure at 150 m shows similar structure to the 50 m flow with no discernable changes in radial speeds (Figure 2b). The maximum inflow is located down-shear, left and to the left of the storm motion. The VWS and storm motion are both directed to the northeast, with the motion lying just to the left of the VWS vector. The flows at 500 m show zero flow within the 50 km radius around the core and the strongest gradients still located to northwest (Figure 2c). The magnitude of the inflow remains constant, while the outflow has increased to 25 m s^{-1} . Analysis of the 1 km radial flow indicates a weakening in both the inflow to the northwest of the center and the outflow due west by 5 m s^{-1} (Figure 2d). The 2 km composite image displays a similar structure as 1 km (Figure 2e). The 3 km analysis shows the outflow maximum located 100 km farther to the southwest than the location at 2 km (Figure 2f). Radar reflectivities confirm the

asymmetric structure with the highest reflectivities located 65 km to the west and 100 km to the north (Figure 3). The south and east portions show reflectivities less than 35 dBZ. Also, there is a radius of maximum winds (RMW) observed on the 500 m tangential plot at a radius of 145 km (Figure 4). The strongest tangential flows are located to the northwest of the LLCC with maximum velocities of 30 m s^{-1} . The tangential field shows strong asymmetries extending over 200 km out from the center. The RMW occupies only the northwest quadrant of the storm. Comparison with the H*wind analysis shows good agreement in the general features with only minor smoothing needed in the northeast quadrant. The H*wind analysis confirms center placement and also shows a secondary wind maximum to the southeast of the center. This maximum is not represented in my analysis as it is located just outside the domain of my data set. Analysis of GPS drops alone would only reveal a wave number one asymmetry in the tangential field instead of the two wave pattern evident in the H*wind analysis. While the composites from the GPS sondes are accurate and provide valuable storm data, they do not provide the whole picture and should be supplemented by additional observations when possible.

Analysis for the following research mission, roughly 24 hours later, shows a more organized TC. The radial flows at 50 m show higher radial velocities, located closer to the core (Figure 5a). There are two inflow maxima; the first is located 123 km to the northeast of the LLCC with -35 m s^{-1} flow. The second, weaker maximum is present in the inner core or 45 km to the northwest of the center with a moderate velocity of -25 m s^{-1} . The inner core, as presented here, is defined to be the annulus within 100 km of the circulation center (Corbosiero and Molinari 2003). This secondary maximum is most

likely a symptom of a convective area based on the low-level convergence situated close to the center. Radar images from the WP-3D aircraft support this hypothesis, as a convective band was observed during reconnaissance with reflectivities equal to or exceeding 35 dBZ (Figure 6). The band followed an arc shape from the inner core maximum out to the stronger maximum. Inflow values are also higher along the convective band, as one would expect and this is also the area where the sharpest gradients are observed. Inflow values to the east of the LLCC averaged -10 m s^{-1} . A small channel of outflow extends from the LLCC to the southwest, with a peak value of 10 m s^{-1} . The inner core maximum strengthens to -15 m s^{-1} on the 150 m plot (Figure 5b). The inflow maxima during this period are located down-shear, left and to the left of the motion vector.

At 500 m, the outer inflow maximum weakens to -25 m s^{-1} , while the flows along the arc and the inner core peak maintain the velocities observed in the lower levels (Figure 5c). The inflow present to the east of the center has also weakened with flows averaging -5 m s^{-1} . Tangential flows at the 500 m level reveal an RMW 60 km from the center with peak velocities of 45 m s^{-1} (Figure 7). The tangential flows again exhibit strong asymmetries with the RMW being located to the northwest of the center. As mentioned in the previous section, this day tangential analysis needed to be smoothed with hand analysis and supplemental data from the H*wind analysis and radar reflectivities. The H*wind analysis again depicts a secondary maximum to the southeast of the center, but it is also located outside of the domain of my data set and is not seen in the tangential composite presented. As noted for the previous analysis period, for the RMW occupies only the northwest quadrant. The flows at 2 km are similar to that of the

lower levels on the first day of analysis (Figure 5d). The inner core inflow maximum has diminished and inflow now increases radially outward towards the northwest. Outflow, averaging 5 m s^{-1} , is observed to the east, south, and southwest of the center. At 2 km, the strong band of inflow is still present to the north-northwest, but outflow averaging 5 m s^{-1} is now present in the northeast quadrant (Figure 5e). Analysis for 3 km shows similar structure as observed at 2 km, but slightly weaker inflow values in the arc to the north-northwest (Figure 5f).

Humberto:

Radial plan view images at 50 m have a wave number 1 asymmetry with inflow from the northeast, outflow to the southwest, and the zero line bisecting the LLCC (Figure 8a). A dipole exists in the radial flow with an inflow maximum of -35 m s^{-1} located 20 km to the northeast of the LLCC and an outflow maximum of 15 m s^{-1} located 40 km to the southwest of the LLCC. Inflow is strongest at 150 m where it reaches a velocity of -40 m s^{-1} (Figure 8b). Reconnaissance radar images reveal that convective cells with reflectivities greater than 40 dBZ formed near the area of maximum inflow and propagated cyclonically around the LLCC (Figure 9). Reflectivities were also weakest in the region of outflow, southwest of the center. Flows in this region, increased to 20 m s^{-1} at 150 m. The low-level inflow maximum is located down-shear, left and to the right of the motion. The effects of this location will be discussed further in the following section.

Analysis of the 500 m radial flows shows a similar structure to the preceding levels with the dipole around the core still evident (Figure 8c). The outflow to the southwest is 20 m s^{-1} and the inflow to the northeast has weakened to -30 m s^{-1} .

Tangential plots at 500 m reveal an RMW at 18 km from the center with velocities reaching 50 m s^{-1} (Figure 10). Plots at 1 km show the continued decrease of inflow, with values only reaching -20 m s^{-1} (Figure 8d). The dipole that is evident in the lower levels has now weakened and is located just to the south of the center and is oriented along a west to east axis (Figure 8e). The southwest outflow region remains constant. Inflow values averaging -5 m s^{-1} were observed to the northeast of the zero line at a height of 3 km (Figure 8f). The slope of the zero line changed little with height and is still bisecting the center from the northwest to the southeast at this level.

Isidore:

The 50 m radial analysis exhibits a weak wave number 1 asymmetry (Figure 11a). The zero line does not divide the flow in half, as observed in Humberto. Rather, the zero line forms an ellipse extending 80 km from the LLCC to the northwest and is approximately 60 km in width. Inside these bounds is an area of outflow, with a peak value of 40 m s^{-1} located 55 km from the LLCC. This maximum is only observed at one point and therefore is not believed to be a larger feature of the TC's structure, rather a convective feature. Since there are no other GPS sondes surrounding this point, the cubic-spline has emphasized this area as a maximum outflow region. I believe the outflow associated with the secondary circulation of the storm to only occupy the region to the northwest of the center, extending out 55 km. Inflow averaging -10 m s^{-1} is observed elsewhere, with a maximum of -20 m s^{-1} situated 15 km to the southeast of the center. Analysis at 150 m shows a similar structure to what is observed at 50 m. The maximum located to the southeast at 50 m has decreased in areal coverage and now occupies a small

region just south of the center (Figure 11b). The highest reflectivities, greater than 40 dBZ, are collocated with the maximum inflow values, based on airborne radar (Figure 12). Reflectivities of 20 dBZ or less, indicative of stratiform rain and weak vertical motions, were observed in the outflow region. The maximum inflow is located down-shear.

Inflow values diminish to an average of -5 m s^{-1} at 500 m and the maximum inflow value to the southeast of the center has also decreased to -10 m s^{-1} (Figure 11c). The region of outflow to the northwest remains constant. An RMW is evident in the 500 m tangential field at a radius of 19 km from the center (Figure 13). There are two tangential wind maxima, the first is located to the north-northwest of the center and the second is located to the south. This analysis is in good agreement with the H*wind analysis and radar reflectivities and required little smoothing. Analysis of the 1 km plan view images reveals the weakest radial flows (Figure 11d). Inflow is only observed in a small area directly south of the core and has a maximum velocity of -10 m s^{-1} . The outflow region has decreased in magnitude and areal coverage. The shape is no longer elliptical and the maximum value of 20 m s^{-1} is located 50 km northwest of the center.

Rita:

The first day of analysis on September 21 exhibited the highest inflow velocity observed during this study. The 50 m radial plot revealed -50 m s^{-1} flow 30 km north of the LLCC (Figure 14a). A small area of outflow with a peak velocity of 5 m s^{-1} is evident along the southeast side of the core. Average inflow values averaging -10 m s^{-1} are observed over the majority of the grid. A pocket of 5 m s^{-1} outflow is located 100 km to

the south east of the center. Radar reflectivities indicate that this point is located in a moat between two spiral rain bands (Figure 15). The outflow is most likely a result of the sinking motion characteristic of a moat. There is also a decrease in the tangential flows in this pocket. At 150 m, the inflow maximum north of the LLCC has decreased to -40 m s^{-1} and a secondary maximum, of equal magnitude, has developed 25 km northwest of the LLCC (Figure 14b). The two pockets of outflow, one in the inner core and another in the moat, remain unchanged. The inflow maxima are located ahead of the storm ahead of the storm motion.

Analysis of the 500 m radial flow shows further degradation of the inflow maximum 28 km to the north with peak values only reaching -30 m s^{-1} (Figure 14c). The secondary maximum to the northwest, has maintained -40 m s^{-1} flows. The pocket of outflow in the inner core has increased to 10 m s^{-1} . Average inflow values have decreased slightly to -7.5 m s^{-1} over the majority of the grid. Tangential flows reveal an RMW at 20 km from the center at this level with a maximum velocity of 80 m s^{-1} to the northwest (Figure 16). Comparison with the H*wind analysis is in good agreement overall and only minor smoothing of the RMW structure was needed. At 1 km, there exists only one inflow maximum 25 km to the northwest of the center with a peak value of -30 m s^{-1} (Figure 14d). Outflow to the southeast has strengthened to 25 m s^{-1} and expanded clockwise so that the zero line extends due west of the storm center. There is a second outflow maximum of 20 m s^{-1} , 30 km to the southwest of the center.

Composites for September 22 reveal similar features to the first day of analysis. The 50 m radial flow shows an inflow maximum 20 km north of the LLCC. Peak velocity in this area is -35 m s^{-1} (Figure 17a). There is also a small pocket of 5 m s^{-1} outflow along

the southeastern edge of the center. Average inflow values over the remaining area are on the order of -10 to -15 m s^{-1} . The inflow at 150 m reveals a more complicated field. A new inflow maximum has formed 45 km to the northwest of the LLCC with peak velocities of -30 m s^{-1} (Figure 17b). The maximum found at 50 m has decreased to -25 m s^{-1} and is still 20 km from the center. There are two other areas of -25 m s^{-1} flow at the same radius; one is to the northwest and the other is to the northeast of the center. These three areas are associated with the inner eyewall and the maximum located 45 km out is associated with the outer eyewall. The NOAA WP-3D lower fuselage radar imagery depicts the presence of concentric eyewalls (Figure 18). The outflow region along the southeast of the core has expanded slightly and increased to 10 m s^{-1} . The maximum inflow velocities and area of greatest convergence is located ahead of the storm motion.

Analysis of the 500 m radial plots shows a weakening in the inflow (Figure 17c). Evidence of the concentric structure can still be seen to the northwest of the center with two maxima at different radii. The peak values have decreased to -20 m s^{-1} for both areas. The outflow to the southeast has expanded but maximum values do not exceed 10 m s^{-1} . The average radial velocity for the remaining area has decreased to -5 m s^{-1} . Tangential plots at 500 m reveal a large RMW (Figure 19). The inner part of the annulus is 15 km from the center. A maximum flow of 70 m s^{-1} is observed to the north of the center in the inner eyewall. The swath of 60 m s^{-1} winds extends radially 60 km to the northwest from the center. By 1 km the inflow has weakened significantly (Figure 17d). There exists a narrow channel of inflow extending 50 km to the northwest from the center. Radial flows in this swath do not exceed -10 m s^{-1} . A broad area of 5 to 10 m s^{-1} outflow is observed directly east and south of the center and radial flows in the remaining area are near zero.

3.2 Vertical Analysis and Inflow Depths

Gabrielle:

Gabrielle, on the first day of analysis, exhibits a rather uniform structure in a layer from 50 m to 1 km. There are no significant changes in the structure of the radial flow and magnitude varies on an order of $\pm 5 \text{ m s}^{-1}$. Even at 2 km the structure still remains fairly similar. Inflow depths of 500 m are observed directly around the core but extend above 3500 m at 200 km to the northwest of the LLCC (Figure 20a). The maximum inflow velocities at 50 m are collocated with the deepest inflow.

Composites from September 16 are also nearly constant with height in the lower levels. The layer of 50 m to 1 km shows no marked change in structure. The largest variations are found along the arc of inflow presented in the previous section where the maximum inflow value is found closer to the core with an increase in height. Inflow depths of 1500 m are present 60 km to the east of the LLCC (Figure 20b). Inflow depths along the arc of higher inflow values, which radar indicated to be a convective band, exceed 3 km. Inflow depth greater than 3 km are also present along the eastern edge of the grid. As discerned in the previous day of analysis, the maximum inflow velocities are coincident with the deepest inflow for the area to the northwest of the center.

Humberto:

In a layer from 50 m to 1 km, the radial flow structure remains nearly constant. The maximum inflow increases to -40 m s^{-1} at 150 m. This increase of 5 m s^{-1} from the 50 m analysis is likely a result of being above the surface layer. At 2 km the inflow field appears slightly skewed to the southeast and the inflow maximum has shifted south so that it is now situated southeast of the center. Inflow depths exceeding 3500 m run

parallel to the east of the zero line (Figure 20c). Inflow depths of 3500 m are coincident with the inflow maximum at 50 m. There are two areas of lower inflow values. The first is located 100 km to the northeast of the LLCC with a depth of 1500 m and the second is located 80 km to the southeast of the LLCC with a depth of 1 km. GPS sonde profiles exhibiting inflow equal to or exceeding 3 km are observed from the edge of the inner core and extend radially outwards. The flow increases in depth as one moves radially out from the core, except in the two regions of lower depths mentioned previously.

Isidore:

Radial flows remain constant between 50 m and 150 m. Average inflow speeds decrease by half between 150 m and 500m and are less than -10 m s^{-1} at 1 km. The outflow feature describe previously maintains a uniform structure from 50 m to 1 km. The outflow magnitude experiences a decrease in velocities by a factor of 2 between 500 m and 1 km. Inflow depths range between 500 and 600 m directly around the core and increase radially outward (Figure 20d). The maximum inflow velocities however, were not collocated with the deepest inflow. The deepest inflow is coincident with the average inflow values found outside of the RMW.

Rita:

For the first day of analysis, the overall radial structure remains unchanged in a layer from 50 m to 500 m. There are variations in of the inflow maxima and the magnitude of the inflow maxima decrease with height, but they do not affect the general structure. At 1 km, both the inflow and outflow maxima have rotated cyclonically by

roughly 30 degrees. The outflow is strongest at this level, and as expected, inflow is weakest. Inflow depths around the core are less than 500 m (Figure 20e). The highest inflow velocities at 50 m have an average inflow depth of 500 m. The deepest inflow values, exceeding 3 km, are located approximately 90 km south of the center. Inflow exceeding 1500 m is observed 100 km to the northeast of the center and 155 km to the north-northwest of the center.

A similar story can be told for September 22. Inflow depths remain less than 500 m around the core (Figure 20f). The strongest inflow values observed in the outer eyewall at 150 m are coincident with the deepest inflow. Depths in this region exceed 1500 m. Depths associated with the inner eyewall have some of the lowest inflow depths observed in this study.

3.3 Harmonic Analysis

Portion of variance calculated on the 50 m radial flow around a circle with a radius equal to the RMW showed a general decrease in the wave number 1 energy with an increase with intensity (Table 3). TS Gabrielle exhibited the highest portion of variance with 78% of the energy contained in wave number 1. The first day of analysis, before Rita developed concentric eyewalls, showed the lowest portion of variance with 71% of the energy represented by wave number 1, as hypothesized. Also, a general decrease in wave number 1 is seen in the distance from the storm center for a particular storm. This shows, for this analysis, that the greatest asymmetries at 50 m are in the vicinity of the RMW, where the surface convergence is strongest.

To better analyze the pattern of asymmetry with increasing intensity, the radial flow at 150 m along the RMW was plotted with respect to the axisymmetric mean (Figure 21). Figure 21 demonstrates that as a TC intensifies the axisymmetric mean strengthens. For the stronger cases, inflow is present around almost all of the RMW, but there are still strong asymmetries present in the radial flow. Therefore, as a TC intensifies, the radial flow appears to become more axisymmetric, however strong gradients are still present even in the strongest case.

	Inside RMW	RMW	1.5 x RMW	2 x RMW	
w1	0.8038	0.7852	0.6712	0.6394	Gabrielle 9/15
w2	0.1750	0.1917	0.2655	0.3032	
w1	0.7006	0.738	NaN	NaN	Gabrielle 9/16
w2	0.1613	0.1648	NaN	NaN	
w1	0.7489	0.7067	0.5674	0.5610	Humberto 9/23
w2	0.1907	0.2148	0.2525	0.2702	
w1	0.7785	0.772	0.7755	0.6689	Isidore 9/21
w2	0.0607	0.0001	0.1623	0.2435	
w1	0.6458	0.7170	0.7978	0.8038	Rita 9/21
w2	0.2513	0.1943	0.0999	0.0941	
w1	0.9033	0.9044	0.8504	0.841	Rita 9/22
w2	0.0014	0.014	0.0434	0.039	

Table 3. Portion of variance for wave number 1 (w1) and wave number 2 (w2) harmonics for each case.

Chapter 4

Discussion

4.1 The Relationship between Motion and VWS

As previous studies have demonstrated, storm motion and VWS both affect the distribution of convection in TCs (Corbosiero and Molinari 2003, Molinari et al. 2006, Raymond 1992, Powell 1982, and Shapiro 1983). If VWS is the main forcing, one would expect to see maximum inflow downshear, left. If storm motion is driving low-level asymmetries then maximum inflow should be located just ahead and to the right of the storm motion. Figure 22 plots the VWS and motion vectors and the predicted regions of maximum inflow for both forces, along with the area of observed inflow. This section will focus on the location of inflow with respect to VWS and motion to determine which mechanism is more dominant in forcing asymmetries.

Gabrielle:

On the first day of analysis for Tropical Storm Gabrielle, the storm motion is 9 m s^{-1} at 59° and the VWS is 14 m s^{-1} heading 43° . The inflow maximum, based upon composite analysis and confirmed by radar reflectivities, is located down-shear, left. This agrees with low-level asymmetries expected from the effects of VWS. Therefore, the VWS may be the primary forcing for the boundary layer asymmetries. The motion may also be affected by the VWS and not just the synoptic pattern. Corbosiero and Molinari (2003) found that when the anticyclonic portion of a vortex is the only part tilted by the shear, then the resulting motion will be to the left of the shear vector. A right of shear motion, as is the case on this day, will result if the cyclonic portion of the vortex is tilted

by the (Dengler and Reeder 1997, Jones 1995). This is suggested to result from a lack of deep convection around the core to counter the effect of the VWS and maintain an upright vortex. Observations measuring hurricane tilt are rare and therefore the aforementioned hypothesis cannot be tested. Since radar reflectivities indicated that deep convection was not present around the core during the composite time, the cyclonic portion of the vortex could be tilted by the presence of the VWS and agrees with the motion to the right of the VWS vector that is observed. Another factor that needs to be considered is the location of Gabrielle with respect to land. Gabrielle was located approximately 145 km off the coast of Florida during this time. Effects due to the proximity to land may have also induced asymmetries due to increased surface friction. Kepert (2006b) concluded that the asymmetries observed in the radial flow for Hurricane Mitch (1998) was due to Mitch being located 80 km off the coast of Honduras. Mitch was moving slowly south and the maximum inflow velocities were located in the northeast quadrant, or left of the motion. Hurricane Mitch's slow motion, however, may have been the reason the increased surface friction affected the storm's structure, since both factors as reasoned by Kepert, were of similar magnitude. This period of analysis for TS Gabrielle, saw a fast motion and high values of VWS and the nearness to land, I believe, may be a negligible factor, but not one that can be ruled out without further analysis.

For the following composite time, September 16, the storm motion is 11 m s^{-1} at 41° and the VWS is 18 m s^{-1} , heading 50° . The inflow maximum is observed down-shear, left, an indication that the VWS may be the dominant factor responsible for the asymmetries. The Best Track reported an increase in maximum sustained winds by 5 m s^{-1} and the MSLP decreased by 5 hPa, as compared with the first day of analysis. The

increase in intensity is interesting as the shear increased by 4 m s^{-1} and the storm should have weakened. The radial composites support the increase in intensity reported with an increase in radial velocities by 20 m s^{-1} in a day. As analyzed in the previous section, the inflow maximum in the inner core indicates that deep convection was located closer to the center. Also, the storm motion was located to the left of shear on this day, leading one to assume that the deep convection closer to the core helped to maintain an upright cyclonic vortex. Reasor and Montgomery (2001) showed that the VWS could intensify a TC if the asymmetries in convection induced by the VWS were stronger than those resulting from a symmetric vortex. Molinari et al. (2006) believe that this is most common during the early stages when the symmetric component is weaker than the asymmetric component. This theory could be the reason why TS Gabrielle intensified under increasing VWS. However, one must also consider the source of the strong VWS, the approaching trough from the northwest. Therefore the intensification could be baroclinically aided, as was found to be the case before TS Gabrielle made landfall on September 14 along the Gulf coast of Florida (Molinari et al. 2006).

Humberto:

Hurricane Humberto has a motion of 8 m s^{-1} , heading 23° and VWS of 10 m s^{-1} , heading 42° . The composites for the radial flows show that the inflow maximum is observed in the inner core and is located down-shear, left and also to the front, right of the motion. Based on this result, both the storm motion and the VWS are perhaps contributing to the wavenumber-1 asymmetry. In the case of TS Gabrielle, the VWS was stronger on both days of analysis and therefore was likely the primary forcing for the

asymmetries. Further studies would be needed to confirm if the magnitude of the inflow maximum is a result of the motion and the VWS working in concert together. This would seem like a plausible scenario by reason that both factors may be forcing convergence into a common region. This would lead to an increase in low-level convergence, compared to a single forcing mechanism, resulting in enhanced convection, ergo increased inflow velocities. The storm motion is located to the left of the shear, suggesting that the deep convection around the core is helping to fight the negative effects of the VWS. The relationship between the motion and the VWS has already been presented, but this analysis raises the question as to at what thresholds will one factor be more dominant than the other.

Isidore:

The relationship between the motion and the VWS is less evident in Hurricane Isidore. The motion is 2 m s^{-1} at 300° and the VWS is 5 m s^{-1} , heading 146° . The maximum inflow is located down-shear, supporting the conjecture that the VWS is the primary factor driving the asymmetry. Two factors are responsible for this: 1) the VWS is of larger magnitude than the motion and 2) the motion is too small to force noticeable convergence ahead of the storm. The magnitude of the inflow maximum is less than that observed in Hurricane Humberto. I believe this to be due to the VWS and motion working in nearly opposite directions. The motion is to the right of the shear, suggesting that the cyclonic part of the vortex is tilted. However, the VWS is weak and the VWS may not be influencing the motion. The negative effect of the VWS on the tilt of the vortex may be supported by the fact that Hurricane Isidore reached maximum intensity

during analysis, attaining sustained winds of 57 m s^{-1} . Nevertheless, the radial composites support the argument that the VWS is strong enough to force boundary layer asymmetries in a major hurricane.

Rita:

During the first composite period, September 21, Rita is moving at 4 m s^{-1} at 283° and the VWS is 3 m s^{-1} , heading 39° . The maximum inflow is ahead of the storm. Therefore, for this case, the primary forcing mechanism may be the storm motion. Even though there is VWS present, it is probably too weak to tilt the vortex and induce the low-level asymmetries in convergence. Also, the translation speed is just below average and deemed strong enough to force convergence ahead of the storm. The motion is oriented to the left of the VWS vector, but as mentioned, the VWS is not strong enough to be responsible for this.

The following composite period shows similar results. Hurricane Rita is moving at 4 m s^{-1} at 300° , and the VWS is 4 m s^{-1} heading 120° . The maximum inflow is located ahead of the storm, supporting the argument that the motion is the primary forcing mechanism. The motion is directly opposite of the VWS, but as mentioned, the shear is believed to be too weak to consider this as a factor influencing the direction of motion.

Chapter 5

Summary and Model Discussion

5.1 Summary

This study consists of composite analyses of Global Positioning System dropwindsonde (GPS sonde) wind observations for 4 TCs of varying intensity. The storms chosen, ranging from tropical storm to category 5 on the Saffir-Simpson scale, are: Tropical Storm Gabrielle (2001), CAT 1 Hurricane Humberto (2001), CAT 3 Hurricane Isidore (2002), and CAT 5 Hurricane Rita (2005).

The goals of this study were to show that 1) as a TC intensifies the inflow becomes more axisymmetric, the magnitude of the radial speed increases, and the depth of the inflow decreases, and 2) the vertical shear of the horizontal wind (VWS) and TC motion are the key factors that force asymmetries in the low-level inflow.

To attain these goals, three different analyses were conducted. The first analysis consisted of producing plan view images of the radial flow relative to the TC center to determine the extent of the asymmetry of this variable at levels of 50 m, 150 m, 500 m, 1 km, 2 km, and 3 km for TS Gabrielle and Hurricane Humberto. Analyses for Hurricanes Isidore and Rita were conducted at 50 m, 150 m, 500 m and 1 km because the aircraft deploying the sondes in these two storms were at a lower altitude. The second analysis was to estimate and plot inflow depth as a function of latitude and longitude from the low-level circulation center (LLCC). These plots were based on the radial flow as a function of height for each GPS sonde. The final analysis was a harmonic analysis of the radial flow for wave numbers 1 and 2 to ascertain what percentage of variance was explained by these wave numbers. Here it was proposed that the total variance from the

wave number 1 asymmetry would decrease with increasing intensity due to the TC becoming more concentric as it matures. The portion of variance was used to quantify the change in asymmetry with an increase in intensity. Radar images from flight reconnaissance were used to support results found in this study.

The radial flow structure at a given height supports the initial hypothesis that higher category TCs are more symmetric. TS Gabrielle and Hurricane Humberto exhibited the strongest wave number 1 patterns in the low-level radial flow, with inflow wrapping around approximately 50% of the core. Plan view images from Hurricanes Isidore and Rita displayed a more axisymmetric field, with inflow wrapping around nearly all of the inner core at 150 m. Both major hurricanes had small areas of outflow located directly upshear. Also, these plan view images revealed that the structure of the radial flow varied little between the top of the surface layer and 1 km height for the two weaker storms, Gabrielle and Humberto. More discernable changes with height in the radial flows were noted between the 50 m and 1 km layer in Hurricanes Isidore and Rita.

There was no correlation found between intensity and the radial speed. However, there appears to be a correlation between the magnitude of the radial speed and the relationship between the VWS and TC motion. For example, the 150 m composites for Rita on September 21 had the highest inflow velocities of -45 m s^{-1} . The maximum was located down-shear, left and to the right of the motion vector. The angle between the VWS and the motion was favorable for both mechanisms forcing asymmetries into the same quadrant, thereby enhancing the inflow speed. On the following day, after Rita experienced a 23 hPa drop in central pressure, the VWS and motion vectors were situated 180° apart resulting in an inflow at 150 m of only -30 m s^{-1} . Another case that this is

valid for is the second day of TS Gabrielle. The TC motion vector was located to the left of the VWS. The angle between them was 16 degrees, less than that observed in Rita, but still placing maximum inflow regions into the same quadrant as predicted by both theories. Gabrielle exhibited inflow velocities of -35 m s^{-1} at 150 m. Evidence that not all major hurricanes would have strong inflow can be shown in Hurricane Isidore's analysis. Composite analysis at 150 m showed the lowest inflow velocities in this study, with maximum speeds of -20 m s^{-1} . The VWS and TC motion angle in this case were opposing each other, possibly leading to lower inflow velocities. The hurricane was still classified as a CAT 5, but the central pressure had risen 17 hPa in 18 hours.

Plots of the depth of the inflow strongly support the hypothesis that inflow depths decrease with intensity within 100 km of storm center, defined here to be the inner core region. Depths observed in TS Gabrielle and Hurricane Humberto exceeded 3 km within the inner core. Hurricanes Isidore and Rita had average inflow depths of 500 m in the inner core. There is evidence of a connection between the deepest inflow depths and the highest 150 m inflow velocities in developing or weak storms. The maximum inflow speeds are coincident with the deepest inflow values near the core for TS Gabrielle and Hurricane Humberto. However, this does not appear to be valid for Hurricane Isidore and the first day of analysis for Hurricane Rita. The highest inflow velocities were collocated with lower inflow depths near the core. The second day of analysis for Rita exhibited deep inflow rates coincident with the highest inflow velocities, located in the new eyewall.

Harmonic analysis performed for each case demonstrated that the portion of variance for wave number 1 decreased with increasing intensity; ergo the energy

occupied by the asymmetric component also decreased leading to an increase in the axisymmetric component. TS Gabrielle contained 78% of the total energy in wave number 1. Hurricane Rita had 6% less, with 72% of the total energy contained in wave number 1. This knowledge can be best applied to the application of initializing a bogus vortex in an operational forecast model. Simulating the boundary layer asymmetries more accurately could improve intensity forecasts in the early stages of a tropical cyclone and will be discussed in the next section.

5.2 Model Discussion

The NHC and the Central Pacific Hurricane Center (CPHC) use multiple tools for analysis and prediction of TCs for their mission to protect life and property. One such tool is the operational forecast models used to predict the track and intensity of TCs. In this section, I will briefly discuss the possibilities of incorporating observed structures composited from GPS sondes in this study to two of the more well-known operational models. The first model is the Geophysical Fluid Dynamics Laboratory (GFDL) coupled hurricane-ocean prediction system developed by NCEP. The GFDL model was introduced operationally in 1995 as the NWS's official hurricane model (Bender et al. 2007). Kurihara et al. (1993) provide a summarized discussion on the details of initializing and filtering the initial vortex. GFDL uses the large-scale global analysis from the Global Forecast System (GFS). The coarse resolution TC in the GFS is removed and replaced with a finer resolution simulated vortex. The vortex is first created using an axisymmetric vortex created by Kurihara et al. (1990) and an asymmetric component is created from that. The asymmetric portion is simulated from the barotropic vorticity equation and truncated at wavenumber-2. Once the asymmetric portion has been simulated it is applied to the top of the boundary layer.

The second operational model is the Hurricane Weather Research and Forecasting model. Full initialization details are given in Gopalakrishnan et al. (2010). This model also begins with the GFS synoptic scale fields and then removes the GFS vortex. An axisymmetric vortex is then used in place of the GFS vortex, which is smoothed to match observed wind radii and MSLP. Perturbations of various fields are also simulated, including horizontal wind anomalies.

The results of this study could be used to better simulate boundary layer structures in model simulations. I concluded that the developmental TC contained a higher percentage of wave number 1 energy than the mature TCs. I think these findings show that the asymmetries in the low-level secondary circulation to be an important factor in intensification and therefore capturing this structure in TC models may improve intensity forecasts. As is now, a one-size-fits-all axisymmetric vortex is tailored to match large-scale observations in operational models. While these models have been shown to improve track errors, they are less successful in decreasing intensity errors (Bender et al. 2007, Gopalakrishnan et al. 2010). Further understanding of the relationship between shear and motion could help improve the asymmetric structure of a TC in model simulations. If the primary forcing for asymmetries is modeled correctly, then the effect that forcing would have on the evolution of the vortex would also be represented better in simulations, possibly resulting in a better intensity forecast.

Chapter 6

Future Work

I concluded in this study that the relationship between VWS and TC motion influences the low-level kinematic asymmetries and the magnitude of the radial speed. Further research is needed to define the thresholds when the VWS will dominate as a forcing mechanism or when TC motion will induce the boundary layer asymmetry. Corbosiero and Molinari (2003) suggested that the motion is just a reflection of the stronger VWS. I hypothesize here that motion would not always be a reflection of VWS because when VWS is weak, the Beta effect and deep layer steering currents would most likely influence the storm motion. I think that VWS and TC motion are separate forcing mechanisms and the VWS will be the dominant force in most cases. When the VWS is weak and the TC motion has a greater magnitude, then the TC motion would be the primary mechanism. For the case when the VWS is weak and the motion is slow, then I hypothesize that the internal dynamics would control the boundary layer asymmetries (i.e. Beta gyres, vortex Rossby waves, diabatic heating).

Model runs using the asymmetries shown in the developing storms in this study should be conducted and compared to current model outputs. I think that effectively simulating the asymmetric vortex in the early stages will improve intensity forecasts. Here I hypothesize that if the model incorporates the deep layer inflow and accounts for the relationship between the VWS and TC motion to force boundary layer asymmetries, then the spin up and intensification of the simulated vortex will be represented better. Forecasters face tougher challenges with highly sheared TCs due to the lack of accurate

model guidance. The results shown in this study may help to forecast low-level asymmetry forcing more realistically, leading to a lower error forecast.

Harmonic analysis conducted in this study demonstrated that almost 80% of the total energy in the developing stages was contained in the wave number 1 harmonic. Ooyama (1982) stated that intensification could not occur without a deep inflow layer to import enough angular momentum into a system to increase rotational velocity. Current forecast models cap the asymmetric portion of the vortex at the top of the boundary layer. However, as was seen in TS Gabrielle and Hurricane Humberto, inflow was present well above the boundary layer; exceeding heights of 3 km. Studies incorporating the aforementioned asymmetries and inflow depths need to be conducted on past storms and compared with current model schemes to determine if the track and intensity forecasts improve.

References

- Bender, M. A., 1997: The effect of relative flow on the asymmetric structure of the interior of hurricanes. *J. Atmos. Sci.*, **54**, 703–724.
- Bender, B.A., I. Ginis, R. Tuleya, B. Thomas, and T. Marchok, 2007: The Operational GFDL Coupled Hurricane-Ocean Prediction System and a Summary of Its Performance. *Mon. Wea. Rev.*, **135**, 3965-3989.
- Black, M.L., J.F. Gamache, F.D. Marks Jr., C.E. Samsury, and H.E. Willoughby, 2002: Eastern Pacific Hurricanes Jimena of 1991 and Olivia of 1994: The Effect of Vertical Shear on Structure and Intensity. *Mon. Wea. Rev.*, **130**, 2291-2312.
- Corbosiero, K. L., 2000: The effects of vertical wind shear and storm motion on the distribution of lightning in tropical cyclones. M.S. thesis, Dept. of Earth and Atmospheric Sciences, University at Albany, State University of New York, 105 pp.
- , and J. Molinari, 2002: The Effects of Vertical Wind Shear on the Distribution of Convection in Tropical Cyclones. *Mon. Wea. Rev.*, **130**, 2110-2123.
- , and ———, 2003: The Relationship between Storm Motion, Vertical Wind Shear, and Convective Asymmetries. *J. Atmos. Sci.*, **60**, 366-376.
- DeMaria, M., 1996: The effect of vertical shear on tropical cyclone intensity change. *J. Atmos. Sci.*, **53**, 2076–2087.
- , and J. Kaplan, 1994: A Statistical Hurricane Intensity Prediction Scheme (SHIPS) for the Atlantic basin. *Wea. Forecasting*, **9**, 209-220.
- Dengler, K., and M. J. Reeder, 1997: The effects of convection and baroclinicity on the motion of tropical cyclone like vortices. *Quart. J. Roy. Meteor. Soc.*, **123**, 699–725.
- Dolling, K., 2010: The Evolution of Hurricane Humberto (2001). PhD. Dissertation, Dept. of Meteorology, University of Hawaii, get page numbers from Klaus!
- Frank, W.M., 1977: The Structure and Energetics of the Tropical Cyclone I. Storm Structure. *Mon. Wea. Rev.*, **105**, 1119-1135.
- , and E.A. Ritchie, 1999: Effects of Environmental Flow upon Tropical Cyclone Structure. *Mon. Wea. Rev.*, **127**, 2044-2061.
- Gopalakrishnan, S., Q. Liu, T. Marchok, D. Sheinin, N. Surgi, R. Tuleya, R. Yablonsky, and X. Zhang, 2010: Hurricane Weather and Research and Forecasting (HWRF) Model scientific documentation. L. Bernardet, Ed., 75 pp.
- Govind, P.K., 1975: Dropwindsonde Instrumentation for Weather Reconnaissance Aircraft. *J. Appl. Met.*, **14**, 1512-1520.

- Heymsfield, G.M., J. Halverson, E. Ritchie, J. Simpson, J. Molinari, and L. Tian, 2006: Structure of Highly Sheared Tropical Storm Chantal during CAMEX-4. *J. Atmos. Sci.*, **63**, 268-287.
- Hock, T.F., and J.L. Franklin, 1999: The NCAR GPS dropwindsonde. *Bull. Amer. Meteor. Soc.*, **80**, 407-420.
- Jones, S. C., 1995: The evolution of vortices in vertical shear. I: Initially barotropic vortices. *Quart. J. Roy. Meteor. Soc.*, **121**, 821–851.
- Kaplan, J. and W.M. Frank, 1993: The Large-Scale Inflow-Layer of Hurricane Frederic (1979). *Mon. Wea. Rev.*, **121**, 3-20.
- , and M. DeMaria, 1995: A simple empirical model for predicting the decay of tropical cyclone winds after landfall. *J. Appl. Meteor.*, **34**, 2499–2512.
- Keper, J.D., 2006a: Observed Boundary Layer Wind Structure and balance in the Hurricane Core. Part I: Hurricane Georges. *J. Atmos. Sci.*, **63**, 2169-2193.
- , 2006b: Observed Boundary Layer Wind Structure and balance in the Hurricane Core. Part II: Hurricane Mitch. *J. Atmos. Sci.*, **63**, 2194-2211.
- Knaff, J.A., S.A. Seseske, M. DeMaria, and J.L. Demuth, 2004: On the Influences of Vertical Wind Shear on Symmetric Tropical Cyclone Structure Derived from AMSU. *Mon. Wea. Rev.*, **132**, 2503-2510.
- Kurihara, Y., M. A. Bender, R. E. Tuleya, and R. J. Ross, 1990: Prediction experiments of Hurricane Gloria (1985) using a multiply nested movable mesh model. *Mon. Wea. Rev.*, **118**, 2185–2198.
- , ——, and R. J. Ross, 1993: An initialization scheme of hurricane models by vortex specification. *Mon. Wea. Rev.*, **121**, 2030–2045.
- Molinari, J., P. Dodge, D. Vollaro, K.L. Corbosiero, and F.D. Marks Jr., 2006: Mesoscale Aspects of the Downshear Reformation of a Tropical Cyclone. *J. Atmos. Sci.*, **63**, 341-354.
- Ooyama, K.V. 1982: Conceptual Evolution of the Theory and Modeling of the Tropical Cyclone. *J. Meteor. Soc. Japan*, **60**, 369-379.
- Peng, M. S., B.-F. Jeng, and R. T. Williams, 1999: A numerical study on tropical cyclone intensification. Part I: Beta effect and meanflow effect. *J. Atmos. Sci.*, **56**, 1404–1423.
- Powell, M.D., 1982: The Transition of the Hurricane Frederic Boundary-Layer Wind Field from the Open Gulf of Mexico to Landfall. *Mon. Wea. Rev.*, **110**, 1912-1932.
- Raymond, D. J., 1992: Nonlinear balance and potential-vorticity thinking at large Rossby number. *Quart. J. Roy. Meteor. Soc.*, **118**, 987–1015.

- , and H. Jiang, 1990: A theory for long-lived mesoscale convective systems. *J. Atmos. Sci.*, **47**, 3067–3077.
- Reasor, P.D., M.T. Montgomery, F.D. Marks Jr., and J.F. Gamache, 2000: Low-wavenumber structure and evolution of the hurricane inner core observed by airborne dual-Doppler radar *Mon. Wea. Rev.*, **128**, 1653-1680
- Riehl, H., and J. S. Malkus, 1961: Some Aspects of Hurricane Daisy 1958. *Tellus*, **13**, 181-213.
- Schneider, R., and G. M. Barnes, 2005: low-Level kinematic, Thermodynamic, and Reflectivity Fields Associated with Hurricane Bonnie (1998) at Landfall. *Mon. Wea. Rev.*, **133**, 3243-3259.
- Shapiro, L.J., 1983: The Asymmetric Boundary Layer Flow under a Translating Hurricane. *J. Atmos. Sci.*, **40**, 1984-1998.
- Sitkowski, M., and G.M. Barnes, 2009: Low-level Thermodynamic, Kinematic, and Reflectivity Fields of Hurricane Guillermo (1997) during Rapid Intensification. *Mon. Wea. Rev.*, **137**, 645-663.
- Wilks, D.S., 2006: *Statistical Methods in the Atmospheric Sciences*. 2nd Ed. Elsevier. 611 pp.

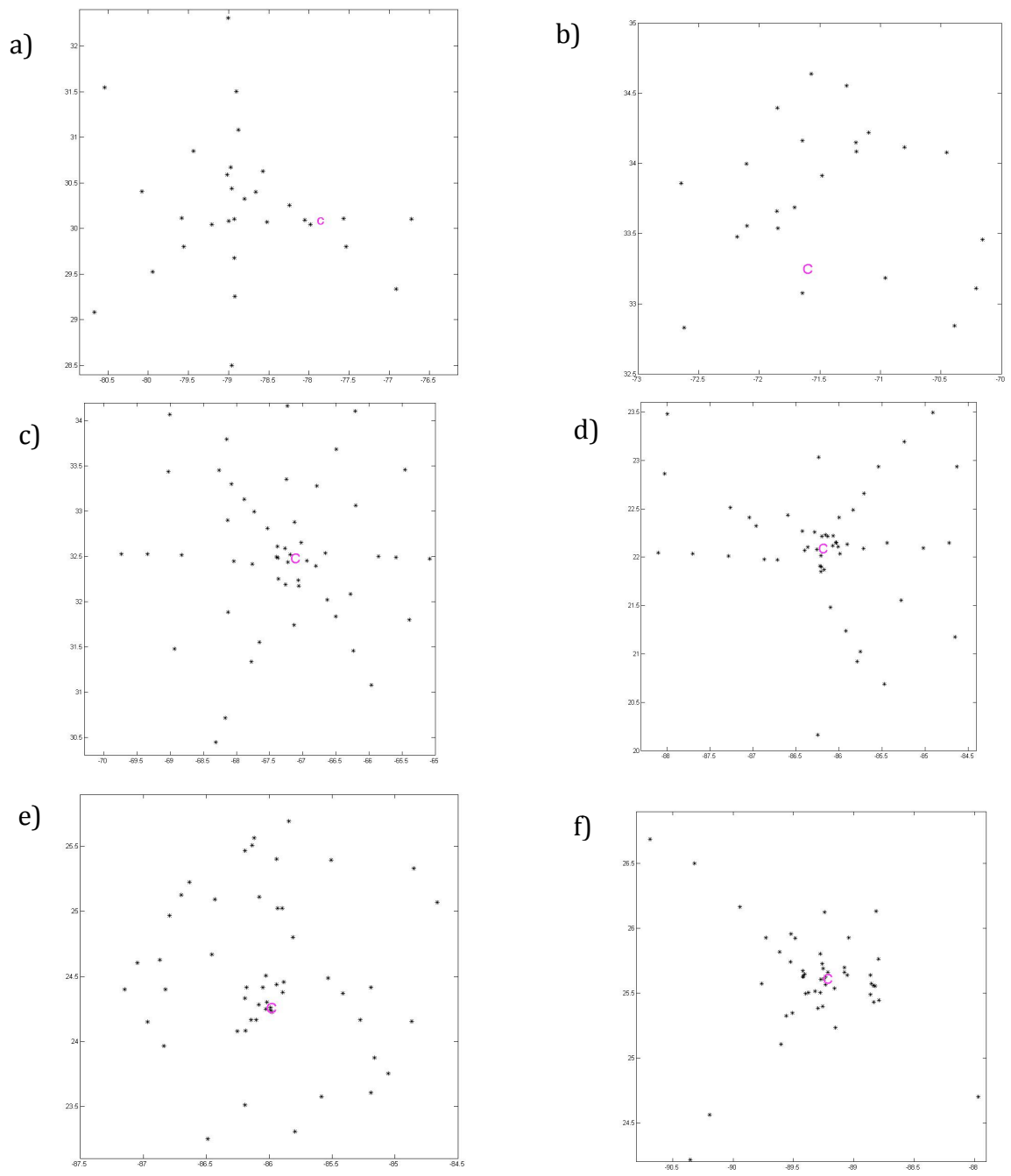


Figure 1. Horizontal Distribution of GPS sondes at 50 m. a) Gabrielle 9/15. b) Gabrielle 9/16. c) Humberto 9/23. d) Isidore 9/21. e) Rita 9/21. f) Rita 9/22.

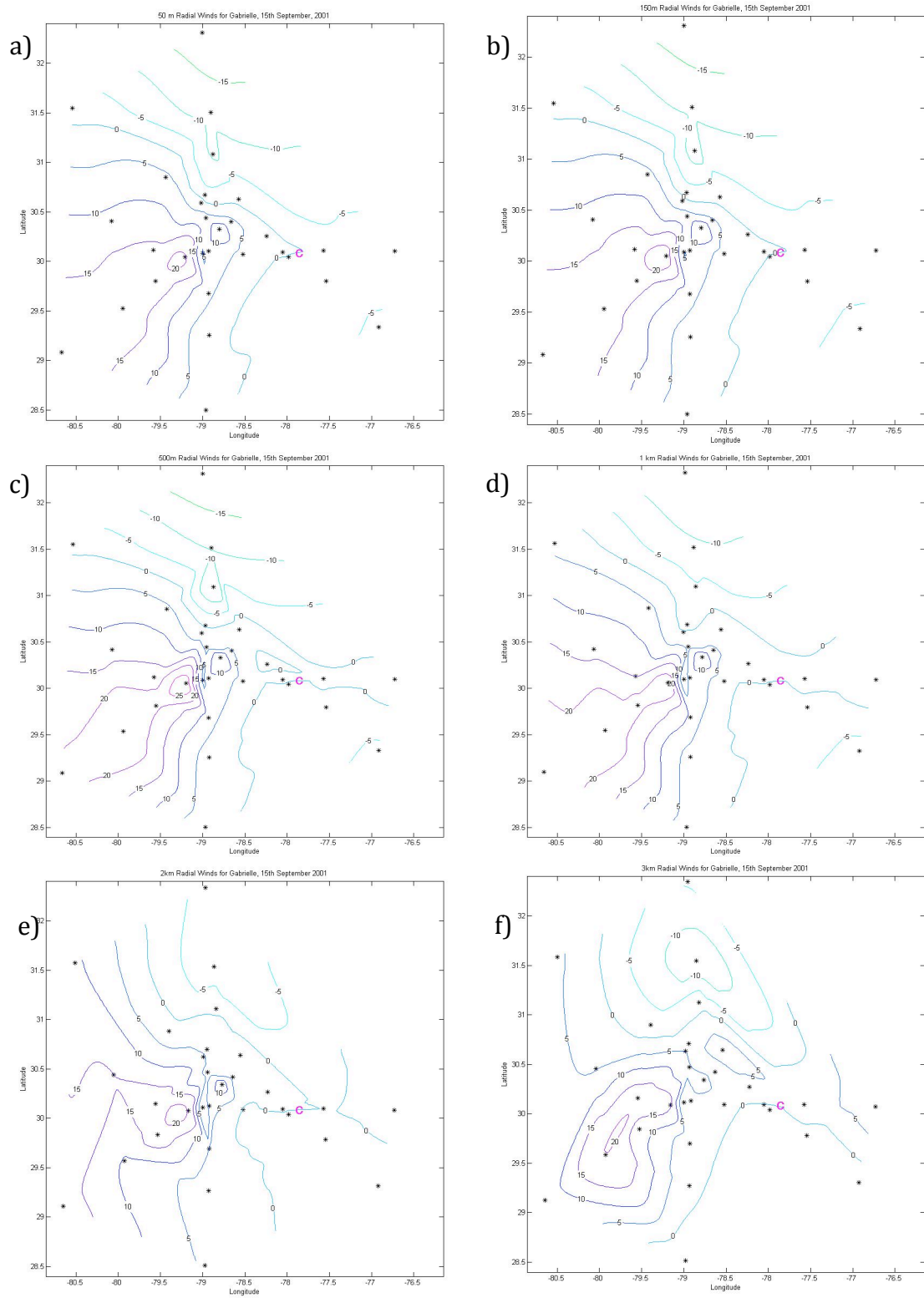


Figure 2. Radial contours (m s^{-1}) for Gabrielle 9/15. * denotes sonde location. a) 50 m b) 150 m. c) 500 m. d) 1 km. e) 2 km. f) 3 km.

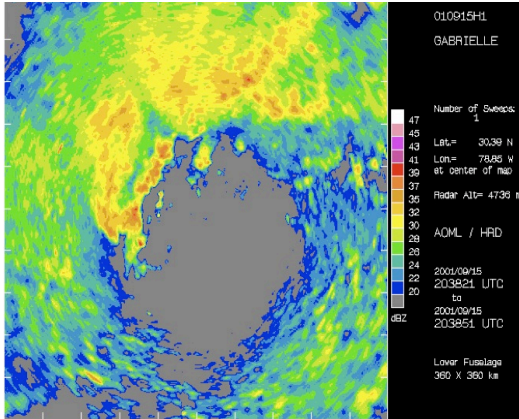


Figure 3. Radar image for Gabrielle 9/15.

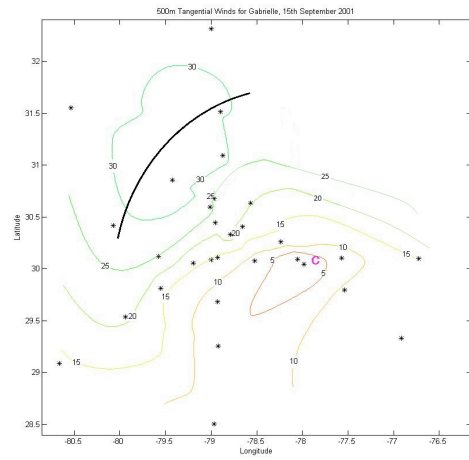


Figure 4. 500 m tangential contours (m s^{-1}) for Gabrielle 9/15. * denotes sonde location. Black circle indicates RMW.

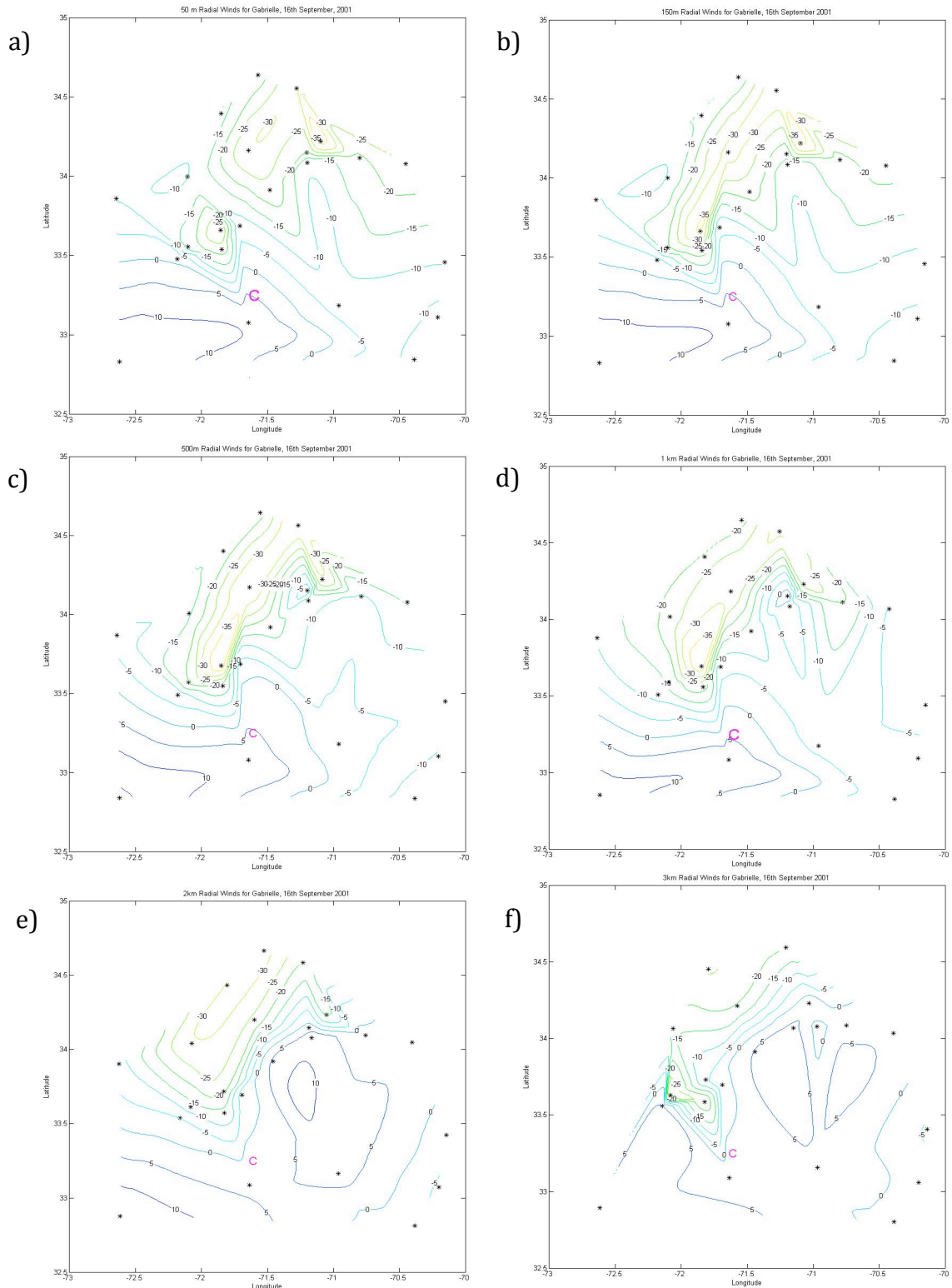


Figure 5. Radial contours (m s^{-1}) for Gabrielle 9/16. * denotes sonde location. a) 50 m b) 150 m. c) 500 m. d) 1 km. e) 2 km. f) 3 km.

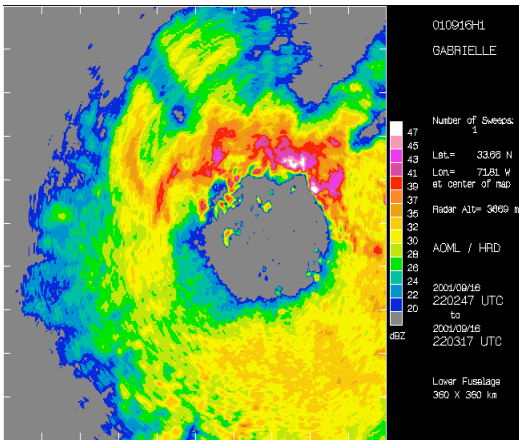


Figure 6. Radar image for Gabrielle 9/16.

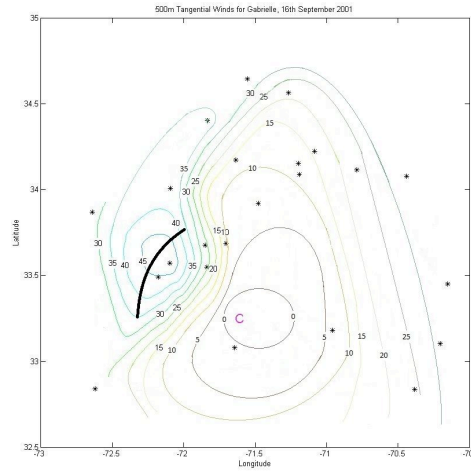


Figure 7. 500 m tangential contours (m s^{-1}) for Gabrielle 9/16. * denotes sonde location. Black circle indicates RMW.

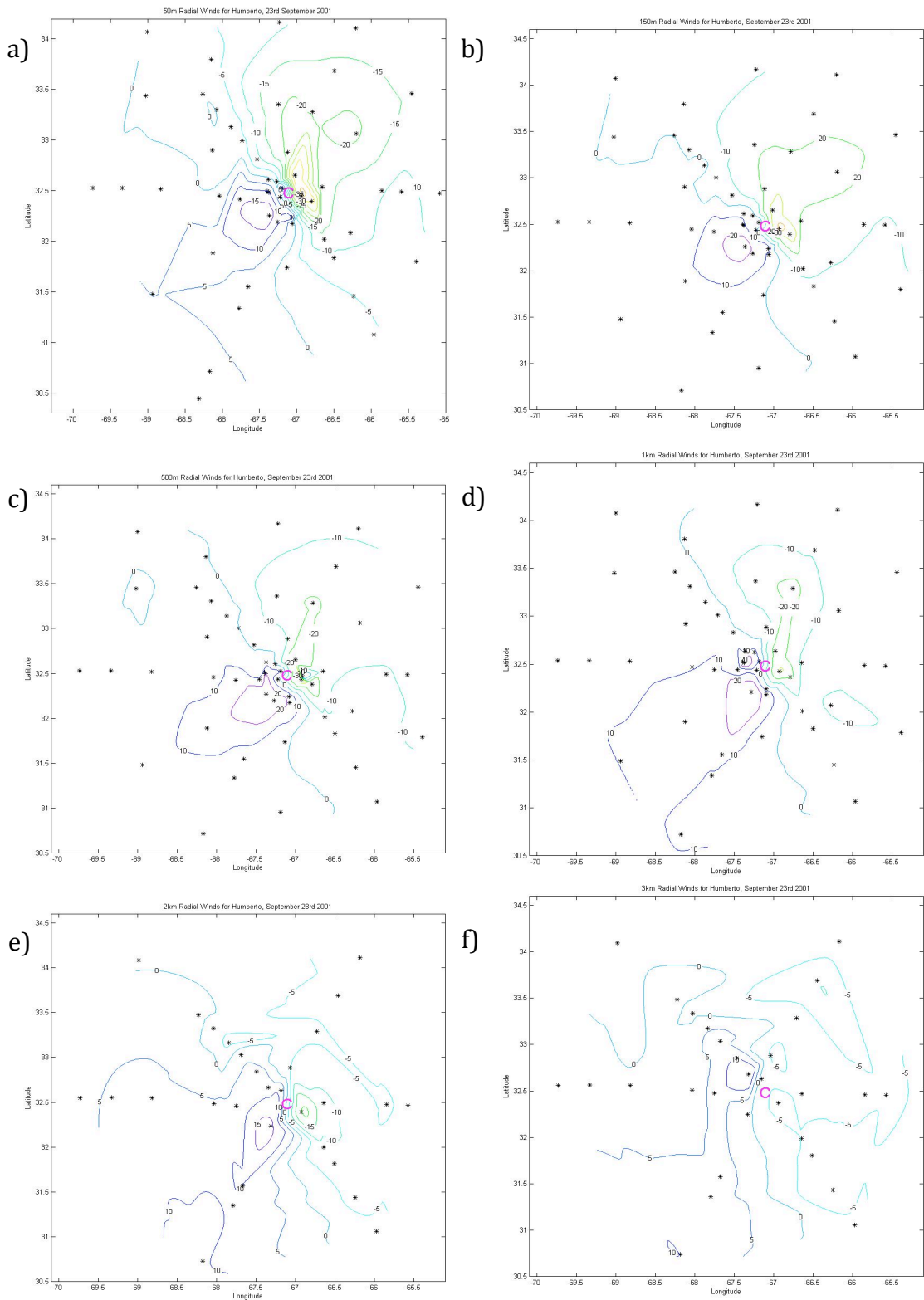


Figure 8. Radial contours (m s^{-1}) for Humberto 9/23. * denotes sonde location. a) 50 m b) 150 m. c) 500 m. d) 1 km. e) 2 km. f) 3 km.

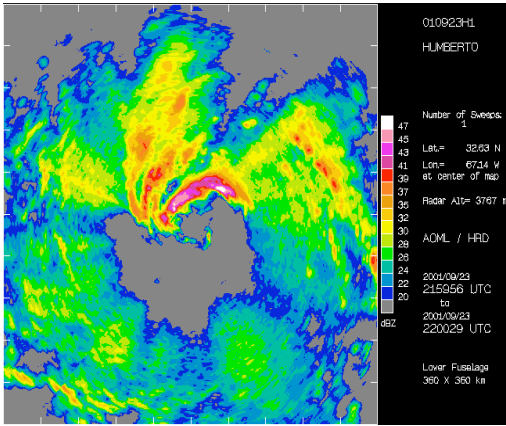


Figure 9. Radar image for Humberto 9/23.

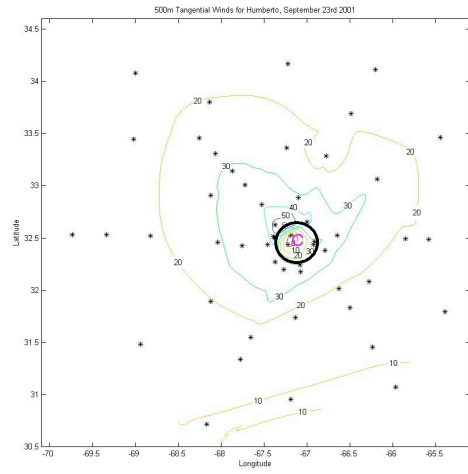


Figure 10. 500 m tangential contours (m s^{-1}) for Humberto 9/23. * denotes sonde location. Black circle indicates RMW.

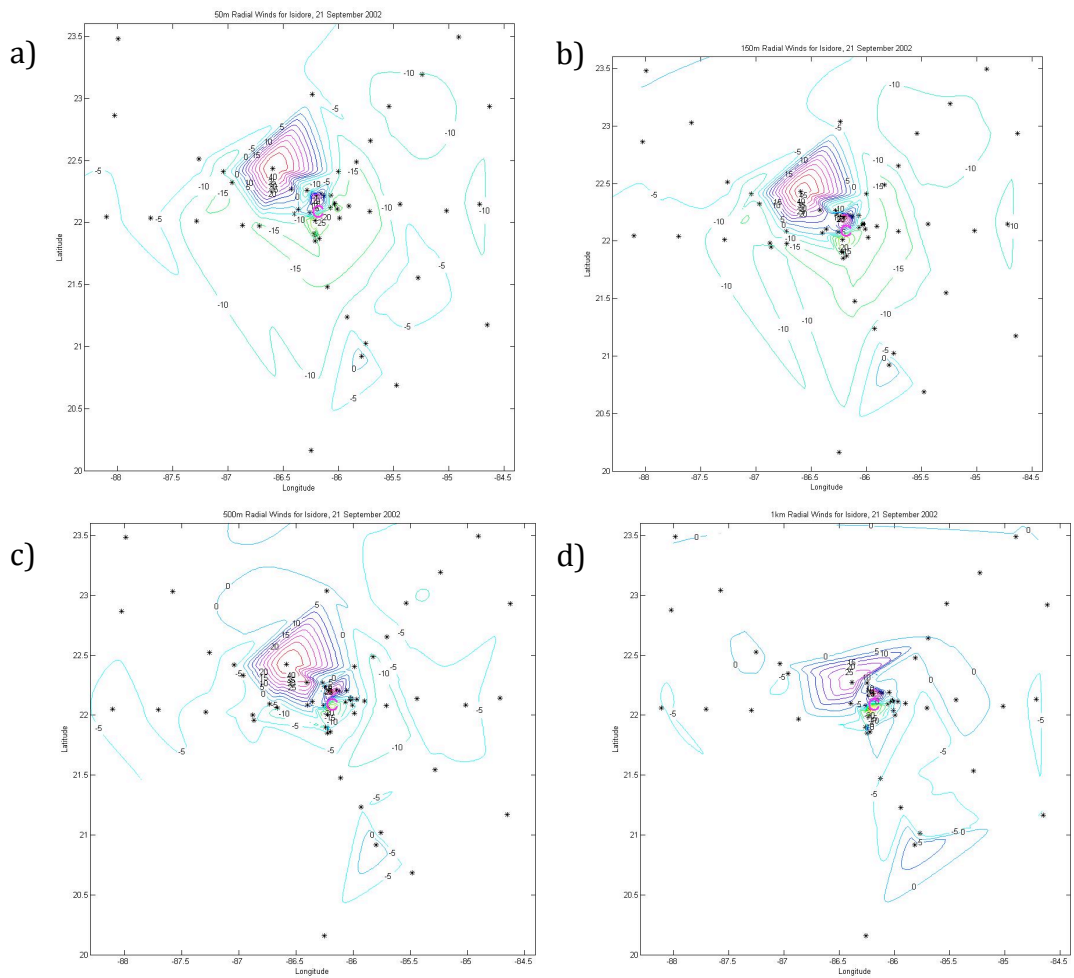


Figure 11. Radial contours (m s^{-1}) for Isidore. * denotes sonde location. a) 50 m b) 150 m. c) 500 m. d) 1km.

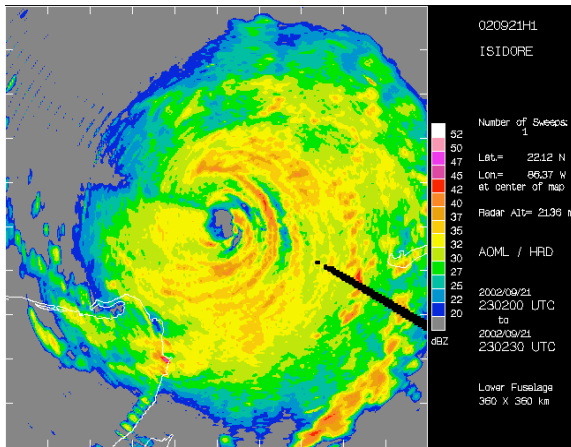


Figure 12. Radar Image for Isidore 9/21.

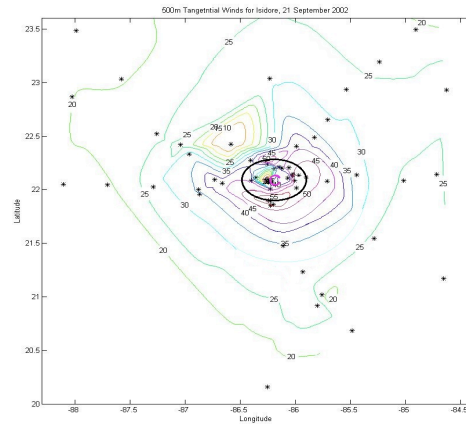


Figure 13. 500 m tangential contours (m s^{-1}) for Isidore 9/21. * denotes sonde location. Black circle indicates RMW.

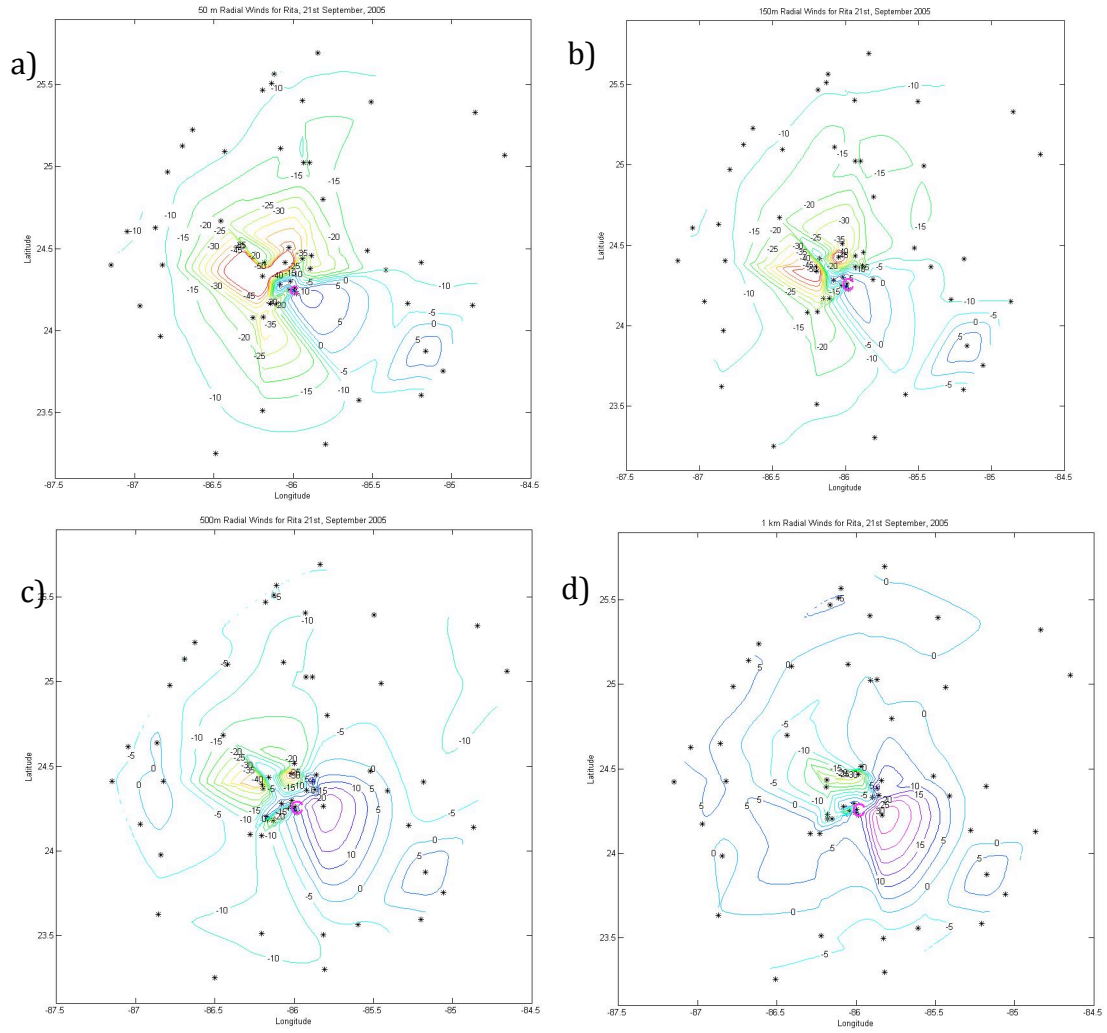


Figure 14. Radial contours (m s⁻¹) for Rita 9/21. * denotes sonde location. a) 50 m b) 150 m. c) 500 m. d) 1km.

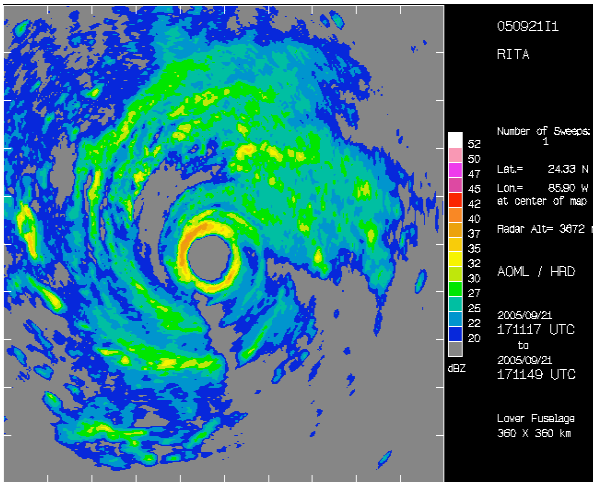


Figure 15. Radar Image for Rita 9/21.

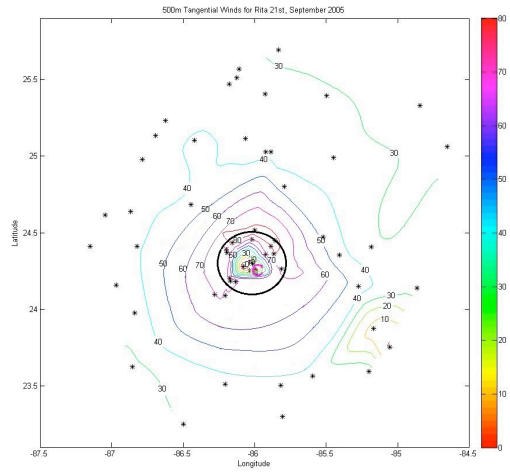


Figure 16. 500 m tangential contours (m s^{-1}) for Rita 9/21. * denotes sonde location. Black circle indicates RMW.

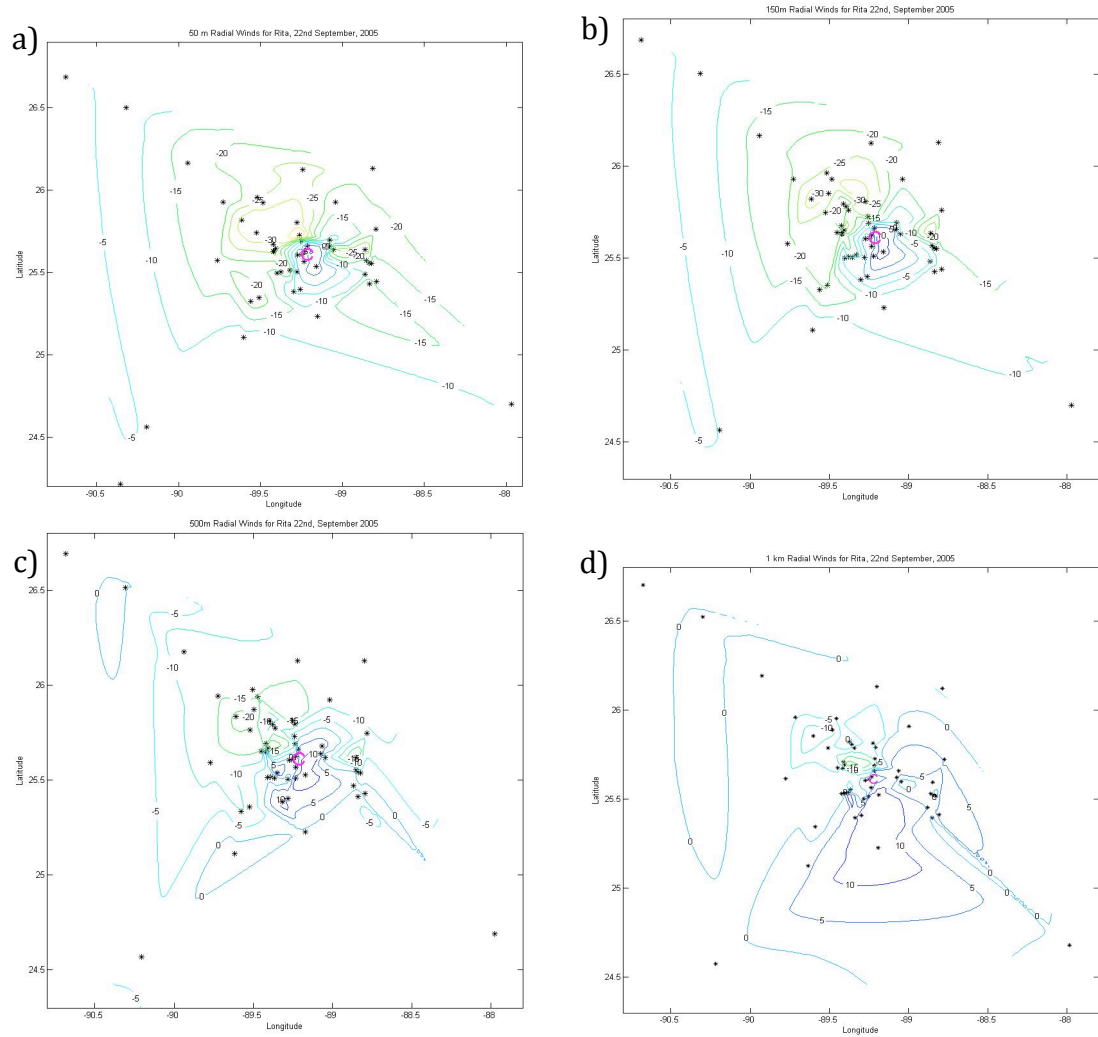


Figure 17. Radial contours (m s⁻¹) for Rita 9/22. * denotes sonde location. a) 50 m b) 150 m. c) 500 m. d) 1 km.

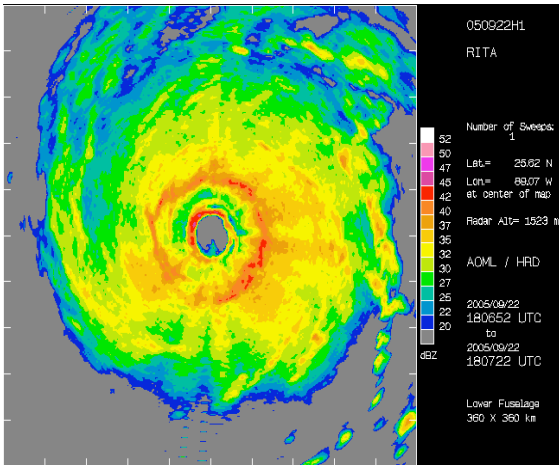


Figure 18. Radar Image for Rita 9/22.

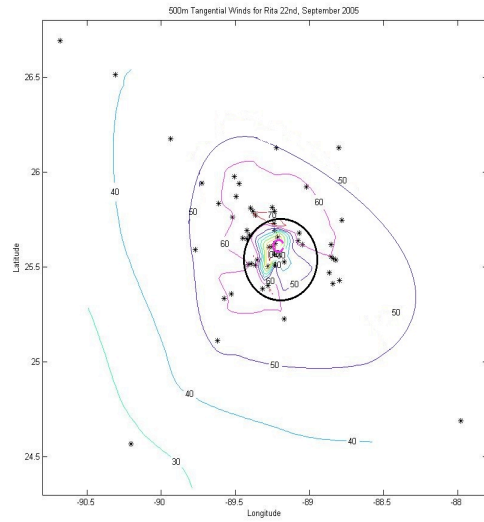


Figure 19. 500 m tangential contours (m s^{-1}) for Rita 9/22. * denotes sonde location. Black circle indicates RMW.

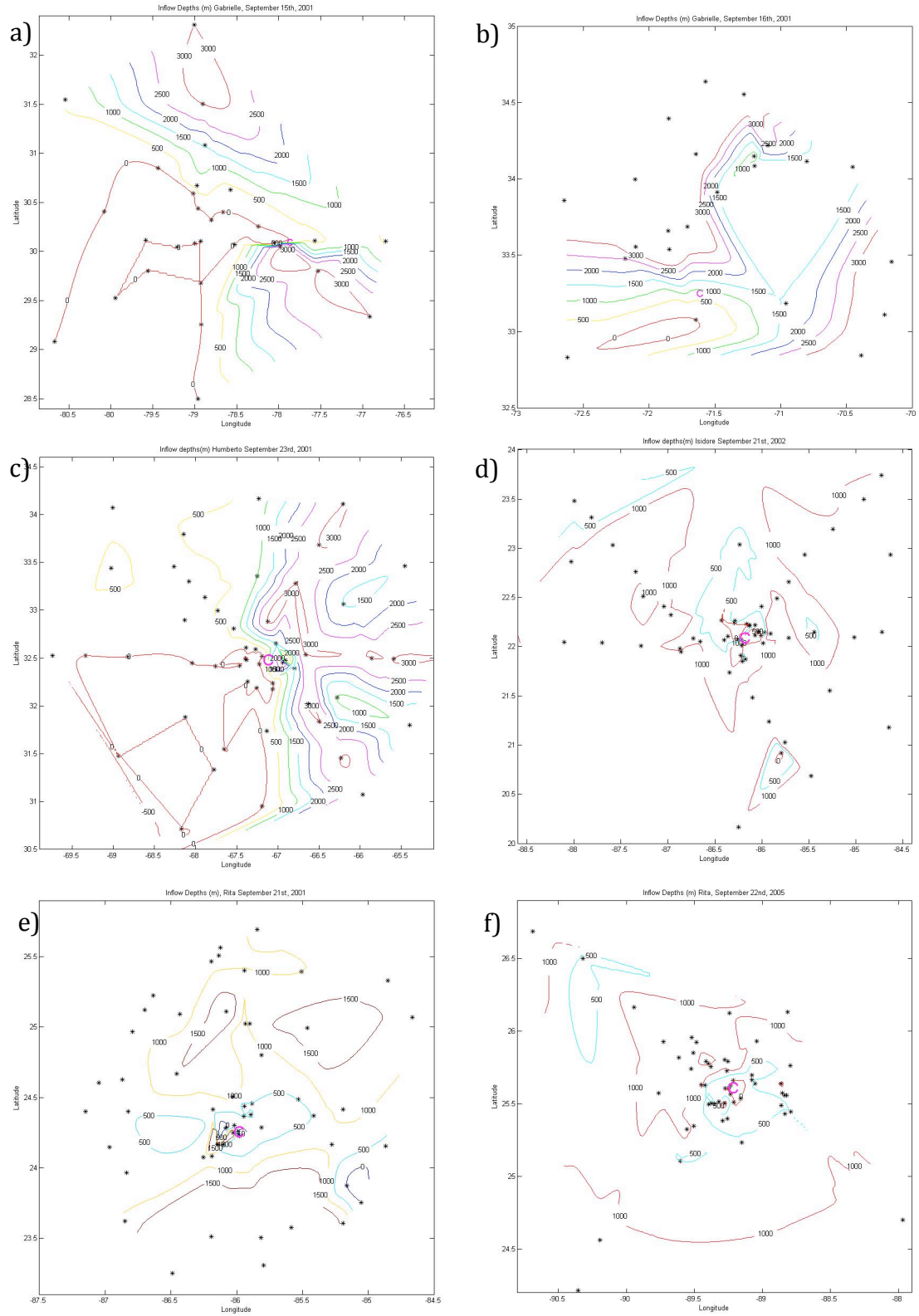


Figure 20. Inflow depths (m) a) Gabrielle 9/15. Outflow is denoted by 0 m. b) Gabrielle 9/16. c) Humberto 9/23. d) Isidore 9/21. e) Rita 9/21. f) Rita 9/22

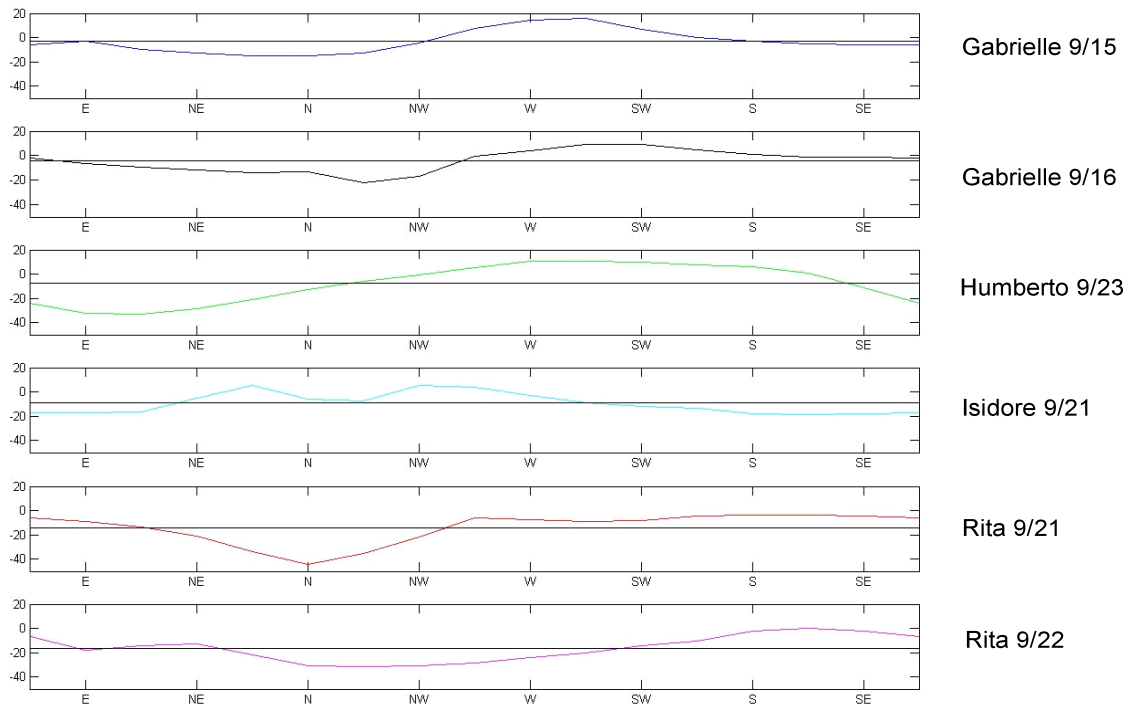


Figure 21. Radial flow around the RMW at 150 m. Solid line is the axisymmetric mean for the radial flow around the RMW.

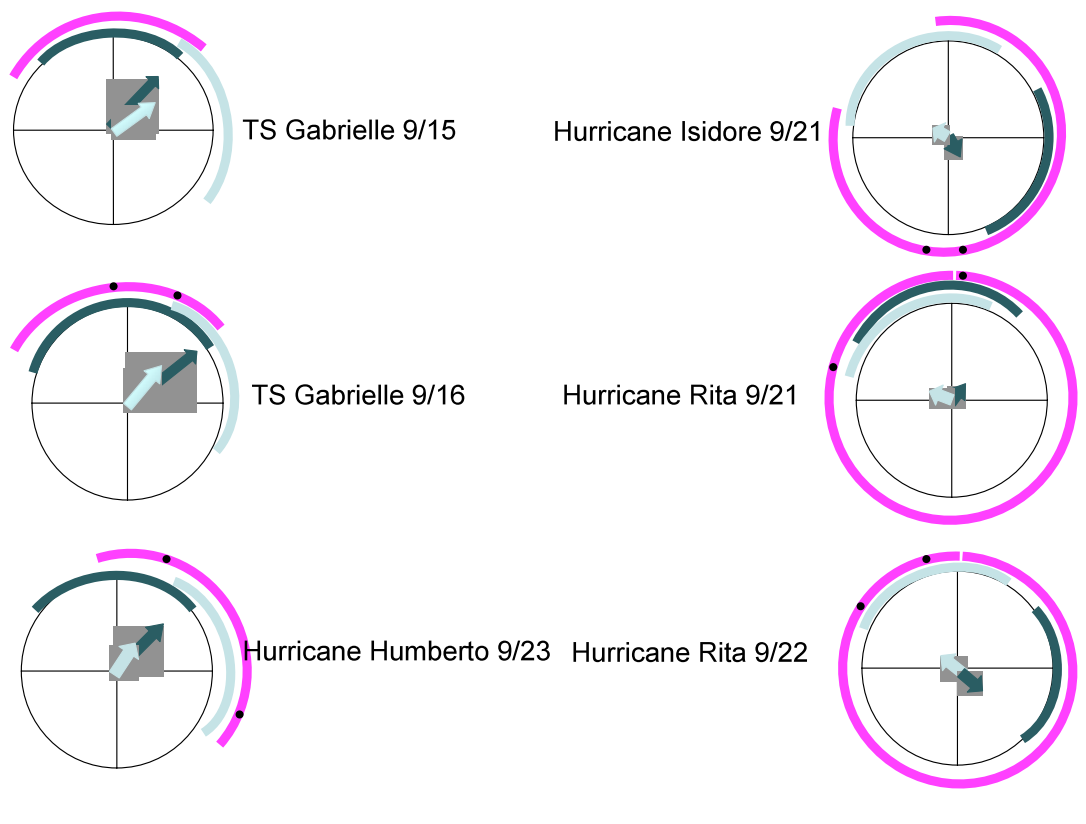


Figure 22. Inflow relative to the VWS and Motion vectors. Range ring indicates 20 m s^{-1} velocity. Light blue arrow marks magnitude and direction of TC motion vector. Light blue arc indicates area of maximum inflow predicted by motion forcing. Dark teal arrow marks VWS magnitude and heading. Dark teal arc indicates area of maximum inflow predicted by VWS forcing. Pink arc represents azimuthal extent of -10 m s^{-1} or greater inflow. Inflow region exceeding -25 m s^{-1} denoted by black dots.